

# Dental evidence for extended growth in early *Homo* from Dmanisi


<https://doi.org/10.1038/s41586-024-08205-2>

Received: 8 September 2023

Accepted: 11 October 2024

Published online: 13 November 2024

Open access

 Check for updates

Christoph P. E. Zollikofer<sup>1,2✉</sup>, Vincent Beyrand<sup>1,3</sup>, David Lordkipanidze<sup>4,5</sup>, Paul Tafforeau<sup>3✉</sup> & Marcia S. Ponce de León<sup>1,2✉</sup>

Human life history is characterized by an extended period of immaturity during which there is a disjunction between cerebral and somatic growth rates<sup>1</sup>. This mode of ontogeny is thought to be essential for the acquisition of advanced cognitive capabilities in a socially complex environment while the brain is still growing<sup>2</sup>. Key information about when and how this pattern evolved can be gleaned from the teeth of fossil hominins because dental development informs about the pace of life history<sup>3–5</sup>. Here we show that the first evolutionary steps towards an extended growth phase occurred in the genus *Homo* at least 1.77 million years ago, before any substantial increase in brain size. We used synchrotron phase-contrast tomography<sup>6</sup> to track the microstructural development of the dentition of a subadult early *Homo* individual from Dmanisi, Georgia. The individual died at the age of  $11.4 \pm 0.6$  years, shortly before reaching dental maturity. Tooth growth rates were high, similar to rates in living great apes. However, the Dmanisi individual showed a human-like delayed formation of the posterior relative to the anterior dentition, and a late growth spurt of the dentition as a whole. The unique combination of great-ape-like and human-like features of dental ontogeny suggests that early *Homo* had evolved an extended growth phase before a general slow-down in life history, possibly related to biocultural reproduction<sup>7</sup> rather than brain growth.

Humans exhibit several aspects of life history different from great apes, such as helpless newborns, early weaning and allomaternal infant care, a prolonged postnatal brain growth period, delayed somatic maturation, late onset of reproduction, transgenerational co-operation and a long post-reproductive life<sup>1</sup>. In particular, humans have an extended period of immaturity called childhood—the time after weaning and before the attainment of nutritional independence—that is characterized by (allo)parental care and ample opportunities for social learning<sup>8</sup>. These traits do not fossilize, however, so inferences on the evolution of human life history must be drawn from developmental proxies preserved in hominin fossils<sup>4,5,9,10</sup>. Teeth are of special relevance because their crowns and roots grow by the daily incremental deposition of enamel and dentin layers, respectively, thus conserving detailed information about the maturation schedule of an individual's masticatory system<sup>5,11</sup>. Humans, compared to great apes, show a marked slow-down in dental maturation, especially of the permanent molars, which correlates well with the pace of cerebral development and somatic maturation across primates<sup>3,5</sup>. Dental incremental growth data from fossil hominins have yielded reliable estimates of the age at death of immature specimens<sup>12</sup>, permitting researchers to use dental growth chronologies to calibrate cerebral, cranial and somatic development. For example, microstructural dental evidence from the immature *Australopithecus afarensis* specimen from Dikika, Ethiopia<sup>13</sup>, obtained using propagation phase-contrast synchrotron microtomography (PPC-SRμCT), suggests that this individual essentially followed an ape-like dental

ontogenetic schedule. However, its endocranial volume (ECV) at the time of death (2.4 years) had reached a smaller proportion of adult ECV than in great apes, which has been interpreted as the first evidence of prolonged postnatal brain growth. There is still relatively little information available on the exact timing of dental ontogeny in early *Homo*. The Nariokotome individual (KNM-WT 15 000), dated to approximately 1.6–1.5 million years ago (Ma), is thought to have followed a great-ape-like rather than human-like dental ontogenetic schedule<sup>14–17</sup>, but these inferences are based on estimates rather than direct measurements of its dental microstructural growth. When exactly the characteristic life-history slow-down occurred in the evolution of our genus *Homo* is therefore still an open question.

Here we present a comprehensive and non-destructive microstructural analysis of dental development in an early *Homo* individual from Dmanisi and draw inferences on the life-history evolution of early *Homo*. The Dmanisi site, dated to 1.85–1.77 Ma (ref. 18), has yielded five well-preserved crania, associated mandibles and various postcranial elements<sup>19–23</sup>. Together with a rich record of faunal remains and lithic artefacts, the Dmanisi ensemble has provided unique insights into the palaeobiology of an early *Homo* population outside Africa, its life history, social organization and cognitive capabilities<sup>24,25</sup>. Here we focus on a subadult individual that is represented by cranium D2700, mandible D2735 and various postcranial elements<sup>20,22</sup>.

The individual's permanent dentition is well preserved, and each tooth type is represented by at least one antimer, except for the lower first

<sup>1</sup>Department of Informatics, University of Zurich, Zurich, Switzerland. <sup>2</sup>IBS Center for Climate Physics, Busan, South Korea. <sup>3</sup>European Synchrotron Radiation Facility, Grenoble, France.

<sup>4</sup>Georgian National Museum, Tbilisi, Georgia. <sup>5</sup>Tbilisi State University, Tbilisi, Georgia. ✉e-mail: zolli@ifi.uzh.ch; paul.tafforeau@esrf.fr; marcias@ifi.uzh.ch

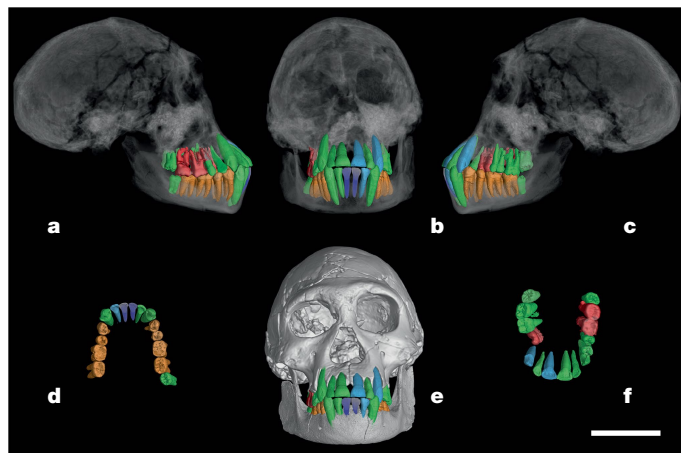


**Fig. 1 | Dentition of Dmanisi skull D2700/D2735.** **a–c**, Computed tomography (CT)-based visualization of the skull and associated teeth showing right lateral (**a**), frontal (**b**) and left lateral (**c**) radiographic projections. **d, f**, Occlusal views of reconstructed mandibular (**d**) and maxillary (**f**) dentition (green, high-resolution PPC-SR $\mu$ CT of isolated teeth used for microstructural analyses; orange, medium-resolution PPC-SR $\mu$ CT of teeth in place, not included in microstructural analyses; red, low-resolution scans (medical CT, not included in analyses); light blue, missing teeth mirrored from preserved antimeres; dark blue, missing mandibular first incisors, reconstructed from second incisors). **e**, Frontal view of the skull. Scale bar, 5 cm.

incisors (Fig. 1). The first molar teeth (M1s) exhibit extensive occlusal wear, resulting in cuspal dentin exposure. The second molars (M2s) only exhibit moderate wear. The lower right third molar (LRM3) was found in isolation, but fits well in its alveolar cavity. The corresponding alveolus for the lower left M3 (LLM3) is not present, indicating LLM3 agenesis<sup>23,26</sup>. The upper right M3 (URM3) exhibits a supernumerary cusp (Extended Data Fig. 1) and was excluded from further microstructural analyses to ensure data consistency, its antimeres having a normal morphology. All M3s exhibit well-developed, but not fully formed, roots, while already exhibiting some wear facets. The individual therefore died before reaching dental maturity, which allows an accurate determination of the individual's age at death through quantification of the incremental growth structures preserved in the tooth enamel and dentin.

We used PPC-SR $\mu$ CT virtual histology<sup>6,27</sup> to track the development of the individual's best-preserved maxillary and mandibular teeth (Fig. 1, Methods, Supplementary Data 1 and Extended Data Fig. 2). To obtain a complete record of dental development, the worn crown cusps were reconstructed using comparative data from better-preserved teeth (Extended Data Fig. 3; Methods). The cusps of the M1 typically comprise the neonatal line (a perinatal stress marker) in their apical-most region. Because this information was lost through dental wear, all following analyses are based on the assumption that the timing of M1 crown initiation was similar to that in living humans and great apes, that is, shortly before, to around, birth (Methods). Following this preparatory work, we reconstructed the developmental profiles of all teeth, as follows (Methods). (1) We identified major stress markers (indicating discrete systemic stress events during development), which are visible as hypoplastic discontinuities in the dental growth line sequences (Fig. 2a and Extended Data Figs. 4–6). Stress lines were matched across all teeth, resulting in a relative chronology of dental development (Fig. 2b). (2) High-resolution (0.72  $\mu$ m voxel size) virtual cross-sections through the best-preserved enamel and dentin regions revealed a long-period (Retzius/Andresen) growth line timing of 6 days (which is at the fast end of variation in fossil hominins, living humans and great apes<sup>28</sup>) (Supplementary Data 2), and an average dentin secretion rate of 4.28  $\mu$ m per day (Supplementary Data 3). (3) We counted the well-preserved long-period growth lines of the dentin (Andresen lines),

and combined this information with the long-period line spacing and the dentin secretion rate data to establish the absolute timing of the major stress events, and of root formation from initiation to completion. (4) These data were combined with stress marker information from the enamel and calibrated with the Andresen line counts in the dentin to reconstruct crown formation from initiation to completion (Extended Data Figs. 4–6). (5) Finally, the crown and root formation schedules of all the teeth were aggregated into a composite record of dental ontogeny from birth to death (Fig. 2b).

Our data indicate that individual D2700/D2735 died at an age of  $11.36 \pm 0.65$  years (the error margin results from interdental variation in the distances between the stress markers, variation in the reconstruction of worn cusps, variation in the assumed M1 crown initiation and variation in the daily dentin secretion rate) (Supplementary Data 1–3). The time to root apex closure of the third molars was estimated to be 1.3–1.5 years (Methods). Thus, D2700/D2735 died shortly before reaching full dental maturity (12.0–13.5 years).

The almost complete incremental growth record of this individual's permanent teeth allowed us to reconstruct the longitudinal ontogenetic trajectory of its dentition from birth to dental maturity (Figs. 3 and 4 and Supplementary Videos 1 and 2). We recorded the ontogeny of D2700/D2735's dentition at 6-month intervals from birth to death and compared this with corresponding data from living humans, great apes and fossil hominins (Methods and Supplementary Data 4). To characterize taxon-specific modes of dental ontogeny, we distinguished between the pattern and rate of permanent dentition formation. The pattern describes how the eight tooth types (I1, I2, C, P3, P4, M1, M2, M3) matured relative to each other (Fig. 3), while the rate describes how the dentition, as a whole, matures with increasing age (Fig. 4). In quantitative terms, the pattern is given by the dental maturation scores (DMSs) of all tooth types of an individual's dentition (with the tooth types indicated by the subscript labels  $DMS_{I1}$ ,  $DMS_{I2}$ ,  $DMS_C$ ,  $DMS_{P3}$ ,  $DMS_{P4}$ ,  $DMS_{M1}$ ,  $DMS_{M2}$  and  $DMS_{M3}$ ), while the rate is given by the DMS of the entire dentition as a function of individual age (Methods).

Figure 3a summarizes the timing of the key dental ontogeny events in humans, chimpanzees and Dmanisi. The intraspecific variation in crown initiation and completion, tooth emergence and root completion is substantial<sup>29–34</sup>. However, a principal component analysis (PCA) of the  $DMS_{I1-M3}$  data (DMS-PCA (ref. 35)) (Methods) showed that humans have a distinctly different pattern of dental ontogeny compared to all great apes (chimpanzees, bonobos, gorillas and orangutans) (Fig. 3b). Notably, the Dmanisi pattern is within the human range of ontogenetic variation and outside the great ape range of variation (Fig. 3b).

Figure 4a shows taxon-specific maturation trajectories of the entire dentition. Chimpanzee dentition matures rapidly during the first few years of postnatal life, reaching full maturity at around 11–13 years of age<sup>36</sup>. Data from gorilla and orangutan specimens of known age suggest trajectories in the upper and lower ranges of the chimpanzee variation, respectively<sup>37,38</sup>. By contrast, human dentition is characterized by a slow early postnatal maturation, reaching full maturity around 18–22 years of age. The dentition of the Dmanisi individual initially followed a slow human-like rate trajectory until approximately 4 years of age, then catching up to reach a chimpanzee-like trajectory around 8 years, and finally reaching dental maturity at 12.0–13.5 years.

Figure 4b shows the inferred instantaneous maturation rate (total DMS per year) along the trajectories. In the chimpanzee dentition, the rate is highest in the first 2 years of postnatal life and then declines towards adulthood. By contrast, in living humans, the rate is comparatively low in the early postnatal period, but then increases to a peak at around 7.0 years of age, after which it declines steadily towards maturity. We refer to the peak rate as the dentition growth spurt (DGS). Notably, the Dmanisi individual also exhibits a DGS, but this occurred at approximately 5.3 years of age, which is significantly later than in chimpanzees (shortly after birth) and close to the lower range of the modern human DGS (in the range 6.0–8.5 years) (Fig. 4b and Extended Data Table 1).

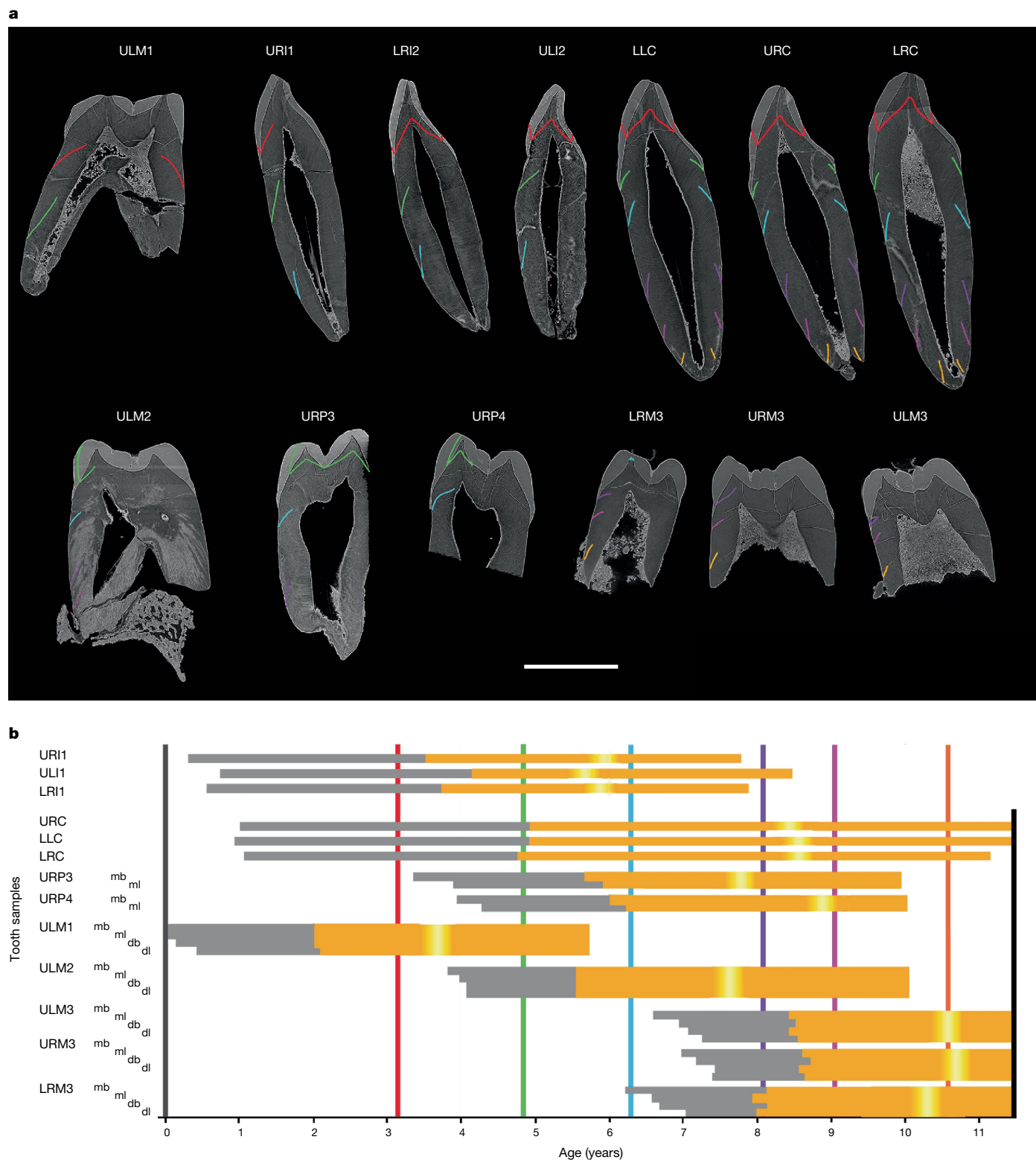


**Fig. 2 | Dental development of the D2700/D2735 individual. a**, PPC-SR $\mu$ CT cross-sectional images through the developmental planes of all analysed teeth (for abbreviations, see text). Coloured lines indicate the six major stress markers (hypoplasias) used for cross-matching the teeth. **b**, Composite chart showing dental development. Tooth abbreviations as in **a**; individual cusps:

mb, mesiobuccal; ml, mesiolingual; db, distobuccal; dl, distolingual. Grey bars, crown formation periods from initiation to termination; orange bars, root formation periods (light bands mark maximum root extension rate as a proxy for dental eruption). The vertical coloured lines correspond to the stress events shown in **a**. Scale bar, 1 cm.

## Discussion

Dmanisi's dental ontogeny appears as a combination of derived human-like and primitive great-ape-like features, on both relative

and absolute time scales. Its pattern of ontogeny is within the range of human variation (Fig. 3b), with a delayed initiation of the posterior teeth (P3, P4, M2, M3, except M1) compared to the anterior teeth (I1, I2, C), and a wide spacing between the M1, M2 and M3 initiation times

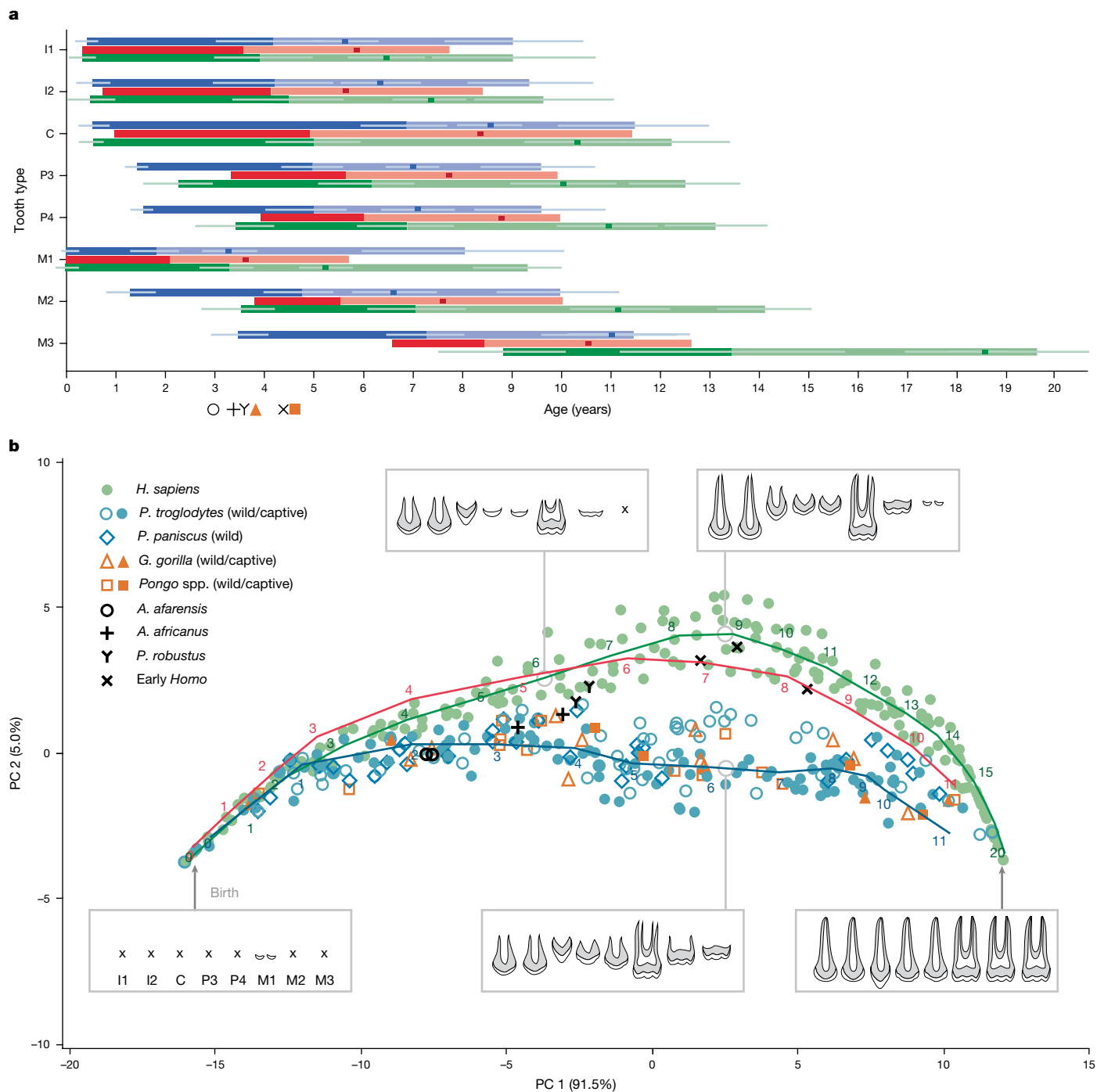


**Fig. 3 | Comparative analysis of patterns of dental ontogeny. a**, Dental ontogenetic schedule by tooth type (Dmanisi, red; humans, green; chimpanzees (captive individuals), blue; dark/light hues indicate crown/root formation periods; small squares indicate estimated eruption time). Error bars ( $\pm 1$  s.d.) drawn at crown initiation and completion, tooth emergence and root completion (data represent  $n = 25$  independent human population-level studies and  $n = 10$  independent studies on chimpanzees; see source data for details). The symbols below the abscissa indicate estimated mean ages at M1 emergence in other great apes (captive gorillas, orange triangle; captive orangutans, orange square) and in fossil hominins (*A. afarensis*, circle; *A. africanus*, + sign; *P. robustus*, Y sign; early *Homo*, × sign). **b**, PCA of dental maturation patterns (DMS-PCA) (Dmanisi, red trajectory; humans, green dots and trajectory; captive known-age

chimpanzees, blue dots and trajectory; numbers on trajectories indicate age in years; wild-living chimpanzees, blue circles; wild-living bonobos, blue diamonds; wild/captive gorillas, open/filled orange triangles; wild/captive orangutans, open/filled orange squares; *A. afarensis*, black circles (Dikika, AL333-105); *A. africanus*, + signs (Sts24, Taung); *P. robustus*, Y signs (DNH107, SK63); early *Homo*, × signs (KNM-ER1590, ZKDB-I4, KNM-WT15000)). Each data point summarizes the maturation states of teeth I1–M3 of a given dentition. Insets show maturation patterns at selected locations in PC space. At comparable ages (6 years), the posterior dentition in humans is delayed compared to chimpanzees. At similar stages of advancement along the ontogenetic trajectory (chimpanzees: 6 years; humans: 9 years), the anterior dentition of chimpanzees appears relatively delayed compared to that of humans<sup>48</sup>. For data sources, see Supplementary Data 4.

compared to great apes (Fig. 3a). As an effect, Dmanisi's dentition, as a whole, matured slowly during the first approximately 5 years of life and exhibited a late DGS (Fig. 4). However, Dmanisi's tooth-specific

maturation rates differed from those of humans in several ways. Once the crowns of the premolars, M2 and M3, were initiated, their formation rates were exceptionally high, resulting in Dmanisi catching up to

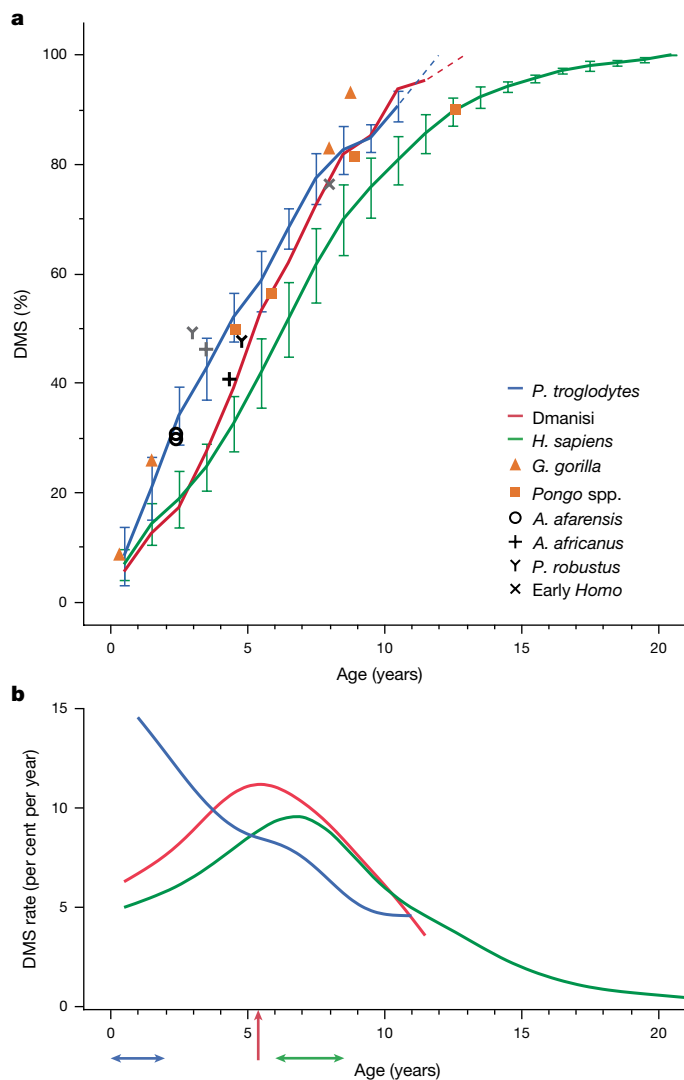


**Fig. 4 | Comparative analysis of rates of dental ontogeny.** **a**, Total DMS versus chronological age. Dmanisi data (red) per year. Chimpanzee data (blue): mean  $\pm$  1 s.d. of 1-year bins ( $n \geq 10$  individuals per bin; Supplementary Data 4). Human data (green): mean  $\pm$  1 s.d. of population-level 1-year bins ( $n = 13$  independent population samples; Supplementary Data 4). Orange symbols indicate known-age individuals of *Gorilla gorilla* (triangles) and *Pongo* spp. (squares). Black/grey symbols indicate fossil hominin specimens of known/estimated individual age. Circles, *A. afarensis* (Dikika 2.4 years and AL333-105 approximately 2.4 years); + signs, *A. africanus* (Taung approximately 3.5 years and Sts24 4.35 years); Y signs, *P. robustus* (SK63 approximately 3 years and DNH107 4.8 years); X signs, early *Homo* (KNM-WT 15000, approximately 8 years). **b**, Inferred instantaneous ontogenetic rate of the dentition (change in total DMS per year) as a function of chronological age. Note early, middle and late timing of DGS (arrows) in chimpanzees (early infancy), Dmanisi (approximately 5 years) and humans (7 years; interpopulation range: 6.0–8.5 years).

a chimpanzee-like maturation trajectory (Fig. 4a), and the estimated eruption times of the molars (M1: around 3.8 years; M2: around 7.6 years; M3: around 10.6 years) being more similar to those observed in wild chimpanzees<sup>31,39</sup> than in humans<sup>40</sup>. Also, the predicted age of dental maturity (around 12.0–13.5 years) is more similar to chimpanzees and other great apes (11–13 years)<sup>36</sup> than to modern humans (18–22 years).

How did Dmanisi's mode of dental ontogeny evolve? Our data suggest a diversity of dental ontogenetic patterns and rates among both fossil hominin and extant great ape taxa. Great apes show a common pattern of ontogeny (Fig. 3b), but taxon-specific differences in rate<sup>38,41</sup>

(Fig. 4a). The data for *A. afarensis* (specimens AL 333-105, Dikika; geological age around 3.3 Ma) and *Australopithecus africanus* (Taung, Sts 24; around 2.8 Ma) suggest that the dental ontogenies of these species were probably within the range of ontogenetic pattern and rate variation seen in extant great apes, whereas *Paranthropus* (DNH 107, SK 63; around 2.0–1.8 Ma) demonstrates a mode of dental ontogeny not found in extant taxa<sup>41,42</sup> (Figs. 3b and 4a). Fossils representing African early *Homo* (KNM-WT 15 000 Nariokotome, KNM-ER 1590; 1.8–1.6 Ma) conform with the Dmanisi/human pattern of ontogeny (Figs. 3b and 4a), supporting the notion that this pattern is an evolutionary hallmark of the genus *Homo*.

What are the implications for the evolution of hominin life history? Because teeth are central to masticatory function, evolutionary changes in their maturation schedules tend to reflect changes in masticatory biomechanics<sup>43</sup> and in the timing of dietary transitions during an individual's life, from breastfeeding to solid foods and from nutritional dependence to independence. These changes, in turn, are thought to reflect evolutionary changes in the allocation of metabolic resources to cerebral, somatic and reproductive maturation, and thus changes in life history.

In Dmanisi, compared to great apes, the characteristically delayed maturation of the posterior permanent dentition (note the relatively late eruption of P3 and P4 in Fig. 3a) and the late DGS imply a prolonged use of the deciduous molars. This probably indicates an extended period of nutritional dependence.

The long childhood period in humans<sup>8</sup> is characterized by delayed dental and somatic maturation relative to brain growth and maturation<sup>3,5,10,44</sup>. This pattern is typically thought to have evolved because the large human brain requires considerably more metabolic energy to grow to adult size than in great apes<sup>2,8,44</sup>. The resulting delay in somatic maturation, in turn, would have provided new opportunities for immature individuals to acquire advanced cognitive skills in a complex social environment while the brain was still growing and maturing<sup>8</sup>.

However, this evolutionary scenario is not applicable to early *Homo*, as the advanced dental and skeletal maturity of Dmanisi and Nariokotome at their respective ages of death are more similar to those of great apes than living humans<sup>22,45–47</sup> (Extended Data Table 2). Furthermore, the brain size of early *Homo* at Dmanisi (ECV range: 546–730 cm<sup>3</sup>) was only moderately larger than that of great apes, and therefore probably had a moderate impact on the metabolic trade-off between brain and body growth.

We therefore propose an alternative scenario for early *Homo* that assumes a diversity of life-history strategies among Plio-Pleistocene hominins, as reflected by the diversity of dental ontogenies<sup>42</sup>. *Australopithecus* probably exhibited a primitive ape-like mode of dental ontogeny<sup>48</sup> (Figs. 3 and 4). However, immature *Australopithecus* individuals show evidence of a prolonged phase of postnatal brain growth and maturation compared to great apes<sup>13,49</sup>, suggesting that this pattern emerged before a marked evolutionary expansion of the brain.

In early *Homo*, according to this scenario, the extended growth phase did not evolve as a consequence of brain expansion and the associated trade-offs in resource allocation<sup>8,10</sup>. Rather, the selective pressures underlying the observed changes must be sought elsewhere. The palaeoanthropological and archaeological context of Dmanisi provides valuable information in this regard. The presence of Mode I stone tools and cut marks on animal bones indicates tool-assisted meat consumption at Dmanisi<sup>18,50</sup>. Therefore, it remains to be investigated whether the evolution of the early *Homo* pattern of dental ontogeny reflects a shift towards tool-assisted meat consumption, implying a reduced overall masticatory load<sup>51</sup>. Furthermore, the sociocultural context and its potential effects on life history and reproduction must be considered<sup>8,52</sup>. The four mature individuals found at Dmanisi<sup>19,21–23</sup> span an age range from early to late adulthood, including one senile individual who had survived several years without teeth<sup>21,24</sup>. The possible presence of post-reproductive individuals in the Dmanisi palaeopopulation<sup>24</sup> can

be viewed in the context of biocultural reproduction<sup>7</sup>, which implies that intergenerational co-operation facilitated an extended period of growth sustained by alloparental provisioning<sup>52</sup>, and ultimately contributed to increased reproductive success.

This raises the question of whether the inferred life-history characteristics of early *Homo* reflect an evolutionary change in reproduction strategies<sup>7,8</sup>—before substantial brain expansion and reorganization<sup>25</sup>, and before a general slow-down in life history. To test these hypotheses, further dental microstructural analyses of key early *Homo* fossils, such as the Nariokotome individual, and of small-brained fossil hominin taxa, such as *Australopithecus sediba*<sup>53</sup> and *Homo naledi*<sup>54</sup>, are required. Overall, our analyses add to the growing body of evidence that the evolution of hominin life histories did not follow a single linear trajectory, but was a branched and modular process, involving diverse selective pressures and adaptive responses.

## Online content

Any methods, additional references, Nature Portfolio reporting summaries, source data, extended data, supplementary information, acknowledgements, peer review information; details of author contributions and competing interests; and statements of data and code availability are available at <https://doi.org/10.1038/s41586-024-08205-2>.

- Robson, S. L., van Schaik, C. & Hawkes, K. in *The Evolution of Human Life History* Vol. 2 (eds Hawkes, K. & Paine, R. R.) 17–44 (School of American Research Press, 2006).
- Leigh, S. R. Brain growth, life history, and cognition in primate and human evolution. *Am. J. Primatol.* **62**, 139–164 (2004).
- Smith, B. H. Dental development as a measure of life-history in primates. *Evolution* **43**, 683–688 (1989).
- Dean, M. C. Tooth microstructure tracks the pace of human life-history evolution. *Proc. R. Soc. B* **273**, 2799–2808 (2006).
- Smith, T. M. Teeth and human life-history evolution. *Annu. Rev. Anthropol.* **42**, 191–208 (2013).
- Tafforeau, P. & Smith, T. M. Nondestructive imaging of hominoid dental microstructure using phase contrast X-ray synchrotron microtomography. *J. Hum. Evol.* **54**, 272–278 (2008).
- Bogin, B., Bragg, J. & Kuzawa, C. Humans are not cooperative breeders but practice biocultural reproduction. *Ann. Hum. Biol.* **41**, 368–380 (2014).
- Bogin, B. Evolutionary hypotheses for human childhood. *Am. J. Phys. Anthropol.* **104**, 63–89 (1998).
- Smith, B. H. & Tompkins, R. L. Toward a life history of the Hominidae. *Annu. Rev. Anthropol.* **24**, 257–279 (1995).
- Schwartz, G. T. Growth, development, and life history throughout the evolution of *Homo*. *Curr. Anthropol.* **53**, S395–S408 (2012).
- Dean, M. C. Retrieving chronological age from dental remains of early fossil hominins to reconstruct human growth in the past. *Phil. Trans. R. Soc. B* **365**, 3397–3410 (2010).
- Smith, T. M. et al. Dental ontogeny in Pliocene and Early Pleistocene hominins. *PLoS ONE* **10**, e0118118 (2015).
- Gunz, P. et al. *Australopithecus afarensis* endocasts suggest ape-like brain organization and prolonged brain growth. *Sci. Adv.* **6**, eaaz4729 (2020).
- Dean, M. C. et al. Growth processes in teeth distinguish modern humans from *Homo erectus* and earlier hominins. *Nature* **414**, 628–631 (2001).
- Dean, M. C. & Lucas, V. S. Dental and skeletal growth in early fossil hominins. *Ann. Hum. Biol.* **36**, 545–561 (2009).
- Dean, M. C. & Smith, B. H. in *The First Humans — Origin and Early Evolution of the Genus Homo*. Vertebrate Paleobiology and Paleoanthropology (eds Grine, F. E., Fleagle, J. G. & Leakey, R. E.) 101–120 (Springer, 2009).
- Dean, M. C. & Liversidge, H. M. Age estimation in fossil hominins: comparing dental development in early *Homo* with modern humans. *Ann. Hum. Biol.* **42**, 415–429 (2015).
- Ferring, R. et al. Earliest human occupations at Dmanisi (Georgian Caucasus) dated to 1.85–1.78 Ma. *Proc. Natl Acad. Sci. USA* **108**, 10432–10436 (2011).
- Gabunia, L. et al. Earliest Pleistocene hominid cranial remains from Dmanisi, Republic of Georgia: taxonomy, geological setting, and age. *Science* **288**, 1019–1025 (2000).
- Vekua, A. et al. A new skull of early *Homo* from Dmanisi, Georgia. *Science* **297**, 85–89 (2002).
- Lordkipanidze, D. et al. The earliest toothless hominin skull. *Nature* **434**, 717–718 (2005).
- Lordkipanidze, D. et al. Postcranial evidence from early *Homo* from Dmanisi, Georgia. *Nature* **449**, 305–310 (2007).
- Lordkipanidze, D. et al. A complete skull from Dmanisi, Georgia, and the evolutionary biology of early *Homo*. *Science* **342**, 326–331 (2013).
- Lordkipanidze, D. et al. A fourth hominin skull from Dmanisi, Georgia. *Anat. Rec.* **288A**, 1146–1157 (2006).
- Ponce de León, M. S. et al. The primitive brain of early *Homo*. *Science* **372**, 165–171 (2021).

- Margvelashvili, A., Zollikofer, C. P. E., Lordkipanidze, D., Tafforeau, P. & Ponce de León, M. S. *Am. J. Phys. Anthropol.* **160**, 229–253 (2016).
- Smith, T. M. & Tafforeau, P. New visions of dental tissue research: tooth development, chemistry, and structure. *Evol. Anthropol.* **17**, 213–226 (2008).
- Hogg, R. et al. A comprehensive survey of Retzius periodicities in fossil hominins and great apes. *J. Hum. Evol.* **149**, 102896 (2020).
- Liversidge, H. in *Patterns of Growth and Development in the Genus Homo* (eds Thompson, J. L. et al.) 73–113 (Cambridge Univ. Press, 2003).
- Smith, T. M., Reid, D. J., Dean, M. C., Olejniczak, A. J. & Martin, L. B. Molar development in common chimpanzees (*Pan troglodytes*). *J. Hum. Evol.* **52**, 201–216 (2007).
- Smith, T. M. et al. Dental development of the Tai Forest chimpanzees revisited. *J. Hum. Evol.* **58**, 363–373 (2010).
- Dean, M. C. & Cole, T. J. Human life history evolution explains dissociation between the timing of tooth eruption and peak rates of root growth. *PLoS ONE* **8**, e54534 (2013).
- Smith, T. M. et al. First molar eruption, weaning, and life history in living wild chimpanzees. *Proc. Natl Acad. Sci. USA* **110**, 2787–2791 (2013).
- Machanda, Z. et al. Dental eruption in East African wild chimpanzees. *J. Hum. Evol.* **82**, 137–144 (2015).
- Boughner, J. C., Der, J. & Kuykendall, K. L. A multivariate approach to assess variation in tooth mineralization using free-lived and captive-raised chimpanzees (*P. troglodytes*). *Am. J. Phys. Anthropol.* **158**, 452–462 (2015).
- Kuykendall, K. L. Dental development in chimpanzees (*Pan troglodytes*): the timing of tooth calcification stages. *Am. J. Phys. Anthropol.* **99**, 135–157 (1996).
- Beynon, A. D., Dean, M. C. & Reid, D. J. Histological study on the chronology of the developing dentition in gorilla and orangutan. *Am. J. Phys. Anthropol.* **86**, 189–203 (1991).
- Smith, T. M. Dental development in living and fossil orangutans. *J. Hum. Evol.* **94**, 92–105 (2016).
- Kelley, J., Schwartz, G. T. & Smith, T. M. Age at first molar emergence in *Pan troglodytes* versus variation in the timing of molar emergence among free-living chimpanzees. *J. Hum. Evol.* **145**, 102823 (2020).
- Haavikko, K. The formation and the alveolar and clinical eruption of the permanent teeth. An orthopantomographic study. *Proc. Finn. Dent. Soc.* **66**, 103–170 (1970).
- Dean, M. C. Measures of maturation in early fossil hominins: events at the first transition from australopithecids to early *Homo*. *Phil. Trans. R. Soc. B* **371**, 20150234 (2016).
- Kuykendall, K. L. in *The Forgotten Lineage(s): Paleobiology of Paranthropus* (eds Constantinou, P. J. et al.) 1–52 (Springer Nature, 2020).
- Glowacka, H. & Schwartz, G. T. A biomechanical perspective on molar emergence and primate life history. *Sci. Adv.* **7**, eabj0335 (2021).
- Kuzawa, C. W. et al. Metabolic costs and evolutionary implications of human brain development. *Proc. Natl Acad. Sci. USA* **111**, 13010–13015 (2014).
- Zollikofer, C. P. E. & Ponce de León, M. S. The evolution of hominin ontogenies. *Sem. Cell Dev. Biol.* **21**, 441–452 (2010).
- Brimacombe, C. S., Kuykendall, K. L. & Nyström, P. Epiphyseal fusion in *Pan troglodytes* relative to dental age. *Am. J. Phys. Anthropol.* **157**, 19–29 (2015).
- Cameron, N., Bogin, B., Bolter, D. & Berger, L. R. The postcranial skeletal maturation of *Australopithecus sediba*. *Am. J. Phys. Anthropol.* **163**, 633–640 (2017).
- Dean, M. C., Lim, S.-Y. & Liversidge, H. M. Patterns of permanent incisor, canine and molar development in modern humans, great apes and early fossil hominins. *Arch. Oral Biol.* **143**, 105549 (2022).
- Falk, D., Zollikofer, C. P. E., Morimoto, N. & Ponce de León, M. S. Metopic suture of Taung (*Australopithecus africanus*) and its implications for hominin brain evolution. *Proc. Natl Acad. Sci. USA* **109**, 8467–8470 (2012).
- Tappen, M., Bukhsianidze, M., Ferring, R., Coil, R. & Lordkipanidze, D. Life and death at Dmanisi, Georgia: taphonomic signals from the fossil mammals. *J. Hum. Evol.* **171**, 103249 (2022).
- Zink, K. D. & Lieberman, D. E. Impact of meat and lower Palaeolithic food processing techniques on chewing in humans. *Nature* **531**, 500–503 (2016).
- Hawkes, K., O’Connell, J. F., Jones, N. G., Alvarez, H. & Charnov, E. L. Grandmothering, menopause, and the evolution of human life histories. *Proc. Natl Acad. Sci. USA* **95**, 1336–1339 (1998).
- Irish, J. D., Guatelli-Steinberg, D., Legge, S. S., de Ruiter, D. J. & Berger, L. R. Dental morphology and the phylogenetic “place” of *Australopithecus sediba*. *Science* **340**, 1233062 (2013).
- Cofran, Z. & Walker, C. S. Dental development in *Homo naledi*. *Biol. Lett.* **13**, 20170339 (2017).

**Publisher’s note** Springer Nature remains neutral with regard to jurisdictional claims in published maps and institutional affiliations.



**Open Access** This article is licensed under a Creative Commons Attribution-NonCommercial-NoDerivatives 4.0 International License, which permits any non-commercial use, sharing, distribution and reproduction in any medium or format, as long as you give appropriate credit to the original author(s) and the source, provide a link to the Creative Commons licence, and indicate if you modified the licensed material. You do not have permission under this licence to share adapted material derived from this article or parts of it. The images or other third party material in this article are included in the article’s Creative Commons licence, unless indicated otherwise in a credit line to the material. If material is not included in the article’s Creative Commons licence and your intended use is not permitted by statutory regulation or exceeds the permitted use, you will need to obtain permission directly from the copyright holder. To view a copy of this licence, visit <http://creativecommons.org/licenses/by-nc-nd/4.0/>.

© The Author(s) 2024

## Methods

### Propagation phase-contrast synchrotron microtomography

Cranium D2700 and associated mandible D2735 were scanned at the ID19 beamline of the European Synchrotron Radiation Facility, Grenoble, France. Volume scans were performed using PPC-SR $\mu$ CT. For general dental morphological assessment, as well as for the counting of Andresen lines, two configurations were used in two successive series of experiments. The first used voxel sizes of 4.89  $\mu$ m with a monochromatic beam set at 51 keV to take advantage of the gadolinium K-edge of the 5- $\mu$ m-thick gadox scintillator. The second series took place a few years later, after substantial technical evolution of the ID19 beamline, and was performed using a 5.06- $\mu$ m voxel size using a polychromatic beam whose spectrum was shaped with a tungsten filter to isolate a peak between the K-edge of the lutecium from the lutecium–aluminium–garnet–(cerium) scintillator (63.3 keV) and the K-edge of the tungsten filter (69.5 keV). This combination enabled much faster scans than with the monochromatic setup due to the higher flux and higher energy, and with perfect beam stability and improved coherence, resulting in much better phase-contrast imaging. In both cases, the propagation distance was 5,000 mm and the scans were performed in half-acquisition to almost double the field of view of the detector. In addition, scans for daily periodicity assessment were performed at 0.75  $\mu$ m at 65 KeV, also in half-acquisition. All scanning parameters are listed in Supplementary Data 1, and a comparison of the monochromatic and polychromatic results is presented in Extended Data Fig. 7.

### Acquisition of dental developmental data

**Determination of developmental planes.** The dental development was tracked based on the PPC-SR $\mu$ CT data of at least one tooth of each type (Supplementary Data 1). Using the software VGStudio Max v.3.4 and later (Volume Graphics GmbH), virtual cross-sections through the teeth were generated to optimally visualize the microstructural growth lines in the enamel (Retzius lines) and dentin (Andresen lines). The optimum cross-sectional plane, named the developmental plane<sup>55</sup>, was defined as the plane passing through a given dentin horn and the top of the underlying pulp cavity. The plane's *x*-axis was oriented in the bucco-lingual direction and its *y*-axis along the tooth's longitudinal axis. The plane's thickness (*z*-axis depth) was set to values between 100 and 150  $\mu$ m. The use of these 'thick sections' enhanced the visibility of the developmental microstructures in the tooth<sup>6</sup>.

**Reconstruction of worn cusp tips.** Several teeth of the Dmanisi individual had undergone substantial wear since eruption, as evidenced by missing enamel cusp tips and dentin horn tips (Extended Data Fig. 3). Because the most relevant microstructural developmental information in the teeth of this specimen came from the dentin (see 'Daily secretion rate'), we focused on reconstructing the relatively small missing apical volumes of the dentin horns (Extended Data Fig. 3), using better-preserved teeth as guides. This process was repeated in several independent sessions. The reconstruction uncertainty inherent in this inference procedure is reflected in the calculations of the dental developmental timing and the age at death (Supplementary Data 1).

**Matching of stress markers across the entire dentition.** The general sequence of tooth development is defined by the order in which teeth initiate, emerge and complete their growth. Episodes of major stress during an individual's development tend to affect the dentition as a whole, resulting in growth discontinuities, which become manifest as stress lines on the outer crown surface and in the microscopic record of enamel and dentin growth lines. A given stress event leaves its mark on all teeth that are still in the enamel and/or dentin deposition phase at this moment. This property is an important prerequisite for placing the development of the individual teeth in a common time frame (Extended Data Fig. 2). In the Dmanisi dentition, six major stress events

could be identified (numbered 1 to 6 in Supplementary Data 1 and assigned different colours in Fig. 2). The matching of these stress lines across all teeth was ensured by cross-correlation between the Retzius and Andresen lines, and was further verified by comparison with the three-dimensional topology of the enamel-dentin junction as well as the hypoplasias of the root surface (Extended Data Fig. 4) and lateral enamel surface (Extended Data Figs. 5 and 6), following the methodology proposed in ref. 56.

**Long-period duration.** The deposition of dental enamel and dentin exhibit both short-term (daily) and long-term (several days) periodicities. In virtual PPC-SR $\mu$ CT cross-sections, the daily incremental growth structures are visible as cross-striations (or laminations) in the enamel (with a size of about 1–3  $\mu$ m)<sup>6</sup>. Typically, the cross-striations are most visible in the relatively flat areas of the mid-lateral cuspal enamel. In enamel, the long-period structures are visible as Retzius lines (size of about 30–40  $\mu$ m, measured along the enamel prisms). The number of daily increments between consecutive Retzius lines gives the value of the long-period line periodicity. This is a property that varies between individuals of a given species (for example, in humans, between 5 and 12 days<sup>28,57</sup>), but can also sometimes vary within a given individual, despite general consensus to the contrary. For example, in a modern human sample of  $n = 40$ , 18 individuals (45%) showed variation in long periodicity, with longer duration in the anterior than the posterior dentition<sup>57</sup>.

To determine the actual long-periodicity of the D2700/D2735 dentition, scans of the enamel at a voxel resolution of 0.72  $\mu$ m were performed on the URP4, URC, ULM3 and LRM3, and the cross-striations were directly traced and counted between the long-period lines (Supplementary Data 1 and 2 and Extended Data Fig. 2). Each tooth was evaluated by two independent observers, and 178 independent measurements were taken all over the teeth. Owing to strong artefacts in the data and the non-perfect preservation of the specimens, periodicities of between 3 and 9 days were observed. The 6-day periodicity represented 41% of the measurements, the 5-day periodicity 31% and the other periodicities 28%. Given the non-normal distribution of these values (Supplementary Data 2) (Kolmogorov–Smirnov test:  $F = 0.2465$ ,  $P < 9.1693 \times 10^{-10}$ ), a Wilcoxon test was performed for comparison with expected periodicities of 5, 6 and 7 days, respectively. The only match between the expected and actual data was observed for the 6-day periodicity ( $P < 0.23$ ), while the results for 5 ( $8.51 \times 10^{-9}$ ) and 7 days ( $7.31 \times 10^{-10}$ ) suggest significant differences between the expected and observed distributions. Our data show no evidence of an antero-posterior gradient in the long-period duration<sup>57</sup>. We thus used the 6-day periodicity to reconstruct the developmental profiles of all teeth by counting the Retzius and/or Andresen lines, and multiplying the total number of lines by the long-period duration.

**Daily secretion rate.** In the D2700/D2735 specimen, the long-period lines in the cuspal enamel (Retzius lines) were barely visible at the available voxel resolution (4.89 and 5.06  $\mu$ m), which prevented direct measurements of the daily enamel secretion rate. However, the D2700/D2735 teeth exhibit exceptionally well-preserved dentin microstructures, which permitted an inference of the daily secretion rates by counting the Andresen lines in those areas where they were clearly visible. Specifically, the daily secretion rate of dentin was evaluated as follows. The length ( $L$ , in microns) of a given well-preserved primary dentin tubule was measured (secondary dentin tends to show compression of the Andresen line patterns), and the number,  $A$ , of the Andresen line intervals along the tubule was counted. The daily secretion rate ( $S$ , in microns per day) was then evaluated as  $S = L/(A \times P)$ , where  $P$  is the periodicity in days (Extended Data Fig. 2). The resulting value of 4.28  $\mu$ m was high compared to humans and chimpanzees<sup>30,58</sup>, but was cross-validated by two observers, and consistent results were obtained when the different sources of information were combined. Finally, this information was combined with the Andresen line counts and

# Article

the cross-matched stress markers—visible in both the enamel and the dentin—to reconstruct the absolute developmental chronology of the whole dentition (Supplementary Data 1).

**Dental eruption time.** The time of dental eruption was estimated from the maximum extension rate of the root, termed the root growth spurt<sup>32,58</sup> (Extended Data Fig. 2). The method used to determine the root extension rates was adapted from previous studies<sup>58,59</sup> and proceeded as follows. Along the cemento-dentin junction, a first 200- $\mu\text{m}$ -diameter circle was placed at the cervix and a second was aligned at the junction between the cemento-dentin junction and the Andresen line, passing tangentially on the side of the first circle (Extended Data Fig. 2). This procedure was repeated all along the length of the root. The greatest distance along the external surface of the root between the two circles marked the maximum extension rate, that is, the root growth spurt.

In great apes, the root growth spurt coincides with the period of dental eruption, whereas in modern humans, the growth spurt precedes eruption<sup>32,58</sup> (Supplementary Data 4). In the Dmanisi individual, therefore, the maximum rates of root growth should be regarded as minimum estimates of tooth eruption times. Furthermore, tooth eruption is a process that takes place over several months. We therefore represent the estimated eruption period as the time point of the maximum root extension rate  $\pm 3$  months (Fig. 2 and Extended Data Fig. 2). It should be noted that such a root growth spurt is visible in the third molars on the last third of the developing roots, while these teeth erupted quite some time before the death of the individual, as indicated by the light wear facets. This supports our basic assumption that the root growth spurt in this individual tends to coincide with the dental eruption.

## Age at death and dental ontogenetic trajectory

**Synopsis of dental development.** The time-calibrated microstructural growth data of the tooth crowns and roots permitted reconstruction of the complete sequence of dental development throughout the life of D2700/D2735, from the initiation to completion of each tooth. The resulting diagram is visualized in Fig. 2 and the underlying data are presented in Supplementary Data 2. These data were used to determine the age at death of the individual, as well as its longitudinal dental ontogenetic trajectory.

**Age at death.** The age at death corresponds to the total time of dental development, from the crown initiation of the first molars (estimated from reconstructions of their worn cusp tips) to the last deposited dentin surface in the roots of the third molars. Because the M1 neonatal line was lost through dental wear, Dmanisi's M1 crown initiation age had to be estimated from comparative data. In humans, the M1 initiation range is from approximately 0.15 years before to approximately 0.03 years after birth, that is,  $-0.06 \pm 0.09$  years (refs. 60,61). With the M1 initiation set to birth (0 years), two independent analyses, performed by P.T. and V.B., yielded an age at death of  $11.42 \pm 0.56$  years (Supplementary Data 1). Adding to this number the M1 initiation range yielded the following upper and lower bounds for the age at death of Dmanisi:  $-0.15 + 11.42 - 0.56 = 10.71$  and  $0.03 + 11.42 + 0.56 = 12.01$  years, which together yield  $11.36 \pm 0.65$  years.

**Estimating the age at dental maturity.** Dental maturity is reached with the root closure of the third molars. The time to root closure in the D2700/D2735 M3s was estimated by comparison with the homologous complete M2 roots. The M3 roots were scaled down to match the size of the M2 roots. Following the M2 dentin tubules, the distance from the open end of the M3 root to the closed M2 root tip was measured. Scaling this distance up to the original M3 size, and assuming an average dentin secretion rate of 4.28  $\mu\text{m}$ , gives 469–561 days (about 1.3–1.5 years) to M3 root completion. The lower and upper bounds for the age at dental maturity are  $10.71 + 1.3 = 12.0$  years and  $12.01 + 1.5 = 13.5$  years.

**Visualization of the ontogenetic trajectory.** The ontogenetic trajectory was visualized using a video capturing the reconstructed developmental stages of each tooth at 6-month intervals, from birth to death, in the form of developmental plane sections (Supplementary Video 1). A second video (Supplementary Video 2) shows the same data in the form of virtual pseudo-orthopantomograms, which can be compared, to some extent, with clinical radiographic orthopantomograms.

The videos were constructed from consecutive virtual snapshots taken at specific time points along the ontogenetic trajectory as follows. Each tooth's developmental plane (as defined above) was used as a base image. On each image, we first annotated the stress lines (Fig. 2 and Extended Data Figs. 4–6), which served as absolute time marks. Using the dentin and enamel extension rates as relative measurements of time, we then interpolated the locations of the Andresen and Retzius lines every 6 months, from birth to death. Then, working backwards from the complete developmental plane, dental material was removed virtually, and the resulting images were saved as snapshots for each 6-month step. The videos were recomposed from the single-tooth image sequences as follows. For each series (upper and lower dentition), two reference lines were defined to determine the position of the teeth before and after emergence, respectively. Pre-emergence teeth were positioned with their distal-most part at the pre-emergence line, while post-emergence teeth were positioned with their proximal-most part (crown cusps) at the post-emergence line. Finally, the images of all the teeth for each time step were merged together, and the timed snapshots were combined to form a video. The effects of tooth wear were not simulated in these videos because it would have been too difficult to make accurate interpolations of this process, so the crowns are shown with reconstructed cusp tips (recognizable by them having higher density than the preserved enamel), and the actual tooth wear is only shown at the time of death.

**Ontogenetic trajectory of the dentition.** The long dental development record of D2700/D2735 up to the subadult stage (well-developed, but open, M3 roots) allowed an almost complete dental ontogenetic trajectory to be reconstructed. The recovery of an individual longitudinal trajectory of 11.4 years is unique for fossil hominins, and even for individuals of living species, where trajectories are typically obtained by combining data from ontogenetic series rather than longitudinal ontogenetic samples. A scoring system developed previously<sup>13</sup> that makes it possible to compare virtual sections with radiographic surveys was used to determine the overall maturation state of the entire dentition at 6-month intervals, from birth to death. Specifically, the maturation state of each tooth (I1, ..., M3) was scored at each time step, following the procedures described in ref. 13. The resulting DMSs (DMS<sub>I1</sub>, ..., DMS<sub>M3</sub>) obtained from the virtual histology sections were then converted into equivalent clinical radiographic scores<sup>13</sup> to permit direct comparisons with the radiographic data from the literature. Finally, at each time step, the DMSs of all the teeth were summed to obtain a total DMS (standardized to 100%). The resulting longitudinal ontogenetic trajectories of D2700/D2735 are visualized in Fig. 3 (DMS<sub>I1</sub>, ..., DMS<sub>M3</sub>) and Fig. 4 (total DMS).

## Comparative data

Comparative data on the developing dentition of known-age chimpanzees and humans were collected from the literature (Supplementary Data 4). The data for chimpanzees were from refs. 35,36,62 and comprise all eight permanent tooth types (I1–M3). The known-age human dataset was combined from studies examining all eight teeth (I1–M3) (refs. 40,63–65) or seven teeth (I1–M2) (refs. 63,65–73). Comparative data for *Pan paniscus* came from ref. 74. The data for *Gorilla* and *Pongo* were acquired from medical CT scans of collection specimens (Supplementary Data 4 and ref. 38). Data on the dental ontogeny of fossil hominin specimens representing *Australopithecus*, *Paranthropus* and

early *Homo* were collected from the literature<sup>9,12,13,48,75–77</sup>. Comparative data on M1 eruption were from refs. 32,34,38,78.

The primary data used in our comparative analyses were the DMSs of each tooth type (DMS<sub>I1</sub>, ..., DMS<sub>M3</sub>), and of the dentition as a whole (total DMS = sum of DMS<sub>I1</sub>, ..., DMS<sub>M3</sub>). The included studies were based on different dental-imaging methods (dental radiography, CT, synchrotron-based tomography) and used different DMS systems, which required prior calibration and standardization<sup>13,79</sup>. As a common reference, we used the Demirjian DMS system<sup>66</sup>, which subdivides dental maturation into eight stages (four stages each for crown and root formation). The calibration schemes used to convert the 10-, 12- and 14-stage DMS systems to the 8-stage Demirjian system are listed in Supplementary Data 4. All calibrated data were standardized to total DMS = 100% for a fully formed dentition. Consistency checks to ensure the comparability of the data are described in detail further below. These checks show that, after calibration, the potential residual bias due to the use of different imaging methods and different scoring systems did not exceed the natural variation found in 1-year age bins of chimpanzees and/or humans.

### Data analysis

We analysed the ontogeny of the dentition as a whole (hereafter referred to as the dental ontogeny) and focused on two aspects, the ontogenetic pattern and rate.

The ontogenetic pattern of an individual's dentition was given by the set of DMSs of the eight tooth types (DMS<sub>I1</sub>, ..., DMS<sub>M3</sub>). For a sample of  $n$  specimens, which resulted in an  $n \times 8$  DMS matrix. To analyse these multivariate data, we used the approach proposed in ref. 35. Using the software JMP v.15.2 (SAS Institute Inc.), a PCA was performed on the  $n \times 8$  DMS matrix, resulting in eight PCs that accounted for the largest to smallest proportions of the total variance in the sample. Typically, the first few components of a PCA comprise a large proportion of the total variance in the sample, which permits visualization of the relevant patterns of variation in the sample in a low-dimensional subspace.

The DMS-PCA method, as we call it here, made it possible to document variation along and across ontogenetic trajectories and to identify taxon-specific differences between the maturation states of the different tooth types relative to each other (Fig. 3b). Ontogenetic trajectories start with no teeth (0,0,0,0,0,0,0,0) and end with all eight fully formed teeth (1,1,1,1,1,1,1,1), so that, in multivariate space, all trajectories have the same starting point, then diverge, finally converging again to a single end point. Therefore, taxon discrimination is best in the middle of the trajectory.

In our analysis of Fig. 3b, PC1 accounted for variation along the ontogenetic trajectories and was essentially equivalent to the total DMS (PC1 =  $-16.105 + 0.284 \times \text{DMS}$ ;  $R^2 = 0.9999$ ;  $P < 0.0001$ ), as already noted in ref. 35, with PC2 accounting for taxon-specific differences between trajectories. It is important to note that individual age was not part of the DMS-PCA, but served as an external variable to time-stamp taxon-specific trajectories through multivariate space. Therefore, specimens of unknown individual age, such as wild-lived great apes and many hominin fossils, can also be included in the analysis.

While the DMS-PCA method provided a detailed and comprehensive picture of dental ontogenetic patterns, we noted that alternative statistical methods have been used to reach similar conclusions regarding the differences between great ape, human and fossil hominin patterns of dental ontogeny<sup>48,80</sup>.

**Ontogenetic rate.** To quantify the rate at which the dentition of a given individual or taxon developed, the total DMS (sum of DMS<sub>I1</sub>, ..., DMS<sub>M3</sub>) was plotted against age. The resulting total DMS trajectories are visualized in Fig. 4a. Furthermore, to summarize the differences between taxon-specific trajectories, we evaluated instantaneous ontogenetic rates =  $(\text{DMS}(t_i) - \text{DMS}(t_{i-\Delta t})) / \Delta t$ , with  $\Delta t = 0.5$  years (Fig. 4b).

Using MS Excel v.16.16.27 software (Microsoft Office), a moving-average function, comprising time steps  $t_{i-\Delta t}$ ,  $t_i$  and  $t_{i+\Delta t}$ , with  $\Delta t = 0.5$  years, was then applied to level out, to some extent, the discontinuities resulting from the discrete nature of the scoring procedure (Supplementary Data 4). The instantaneous ontogenetic rates trajectory of chimpanzees was evaluated from the data in refs. 35,36,62. The human instantaneous ontogenetic rate trajectories were evaluated per population from the maturation score data for eight teeth<sup>40,63–65,81</sup> or seven teeth<sup>63,65,67–70,72,73</sup>. The human DMS trajectories show a DGS, the timing of which varies between populations (6.3–8.5 years) (see main text and Extended Data Table 1). The upper range (8.5 years) largely coincides with M3 crown initiation, such that seven-teeth scoring schemes are unlikely to bias DGS estimates compared to eight-teeth scoring schemes.

### Consistency checks

**Influence of imaging methods and scoring schemes on dental maturation trajectories.** To assess how different imaging methods and different scoring schemes affected the evaluation of the dental ontogenetic rate and pattern, we used data from two independent studies of dental ontogeny in Finnish children, here named Haavikko70 (ref. 40) and Nyström07 (ref. 82). The Haavikko70 data were based on a ten-stage DMS scheme, whereas the Nyström07 data used the eight-stage Demirjian scheme<sup>66</sup>. To assess the effects of imaging methodology (traditional dental radiography versus tomography-based virtual histology), we recoded the Haavikko70 data from the original radiographic to histological (tomographic) scores, using the conversion scheme presented in ref. 13. To assess the effects of data standardization, we recoded the Haavikko70 data with the ten-to-eight-stage recoding scheme presented in Supplementary Data 4. The analyses presented in Extended Data Fig. 8a,b thus compare four datasets: Nyström07 eight-stage, Haavikko70 ten-stage, Haavikko70 eight-stage radiography and Haavikko70 eight-stage virtual histology. We evaluated the DMS-versus-age profiles (Extended Data Fig. 8a), and used a DMS-PCA to visualize the ontogenetic trajectories through multivariate space (Extended Data Fig. 8b). Then results show that the different scoring schemes yielded different DMS-versus-age profiles, but that standardization led to good correspondence between the two datasets. As noted earlier<sup>12,13,83</sup>, the uncalibrated data from the virtual histology yielded total DMS-versus-age profiles that were consistently more advanced than the radiography-based profiles. Interestingly, however, in the DMS-PCA space, all four datasets (calibrated and uncalibrated) showed dental maturation trajectories that largely coincided, indicating that the DMS-PCA was robust to differences in imaging methods and scoring systems.

**Dental maturation profiles and evaluation of the dentition growth spurt.** To assess the influence of different DMS schemes on the evaluation of the DGS, we compared dental maturation data from three independent studies on Finnish children<sup>40,67,82</sup>. These studies used different scoring schemes (ten-stage versus eight-stage), and different tooth arrays (including/excluding M3) (Extended Data Fig. 8c and Supplementary Data 4). Nevertheless, the DMS rate peaks were at similar locations along the age axis (Extended Data Fig. 8d), indicating that the evaluation of DGS was robust to differences in DMS scoring schemes.

**Assessment of age-related variation in dental maturation patterns along taxon-specific ontogenetic trajectories.** DMS-PCA was performed on known-age humans and chimpanzees. As shown in Extended Data Fig. 8e, there is intra-taxon overlap between the 1 s.d.-density ellipses around consecutive 1-year age groups. The natural variation within 1-year age groups along the trajectories tended to be greater than the potential bias remaining after calibration for different data acquisition and scoring methods (Extended Data Fig. 8b).

## Reporting summary

Further information on research design is available in the Nature Portfolio Reporting Summary linked to this article.

## Data availability

Source data for Figs. 3 and 4 are provided with the paper. The synchrotron data that support the findings of this study are available in the ESRF Palaeontology Database with the following identifiers: <https://doi.org/10.1515/ESRF-DC-1897099374> (<https://paleo.esrf.fr/datasets/1900295870>), <https://doi.org/10.1515/ESRF-DC-1897099382> (<https://paleo.esrf.fr/datasets/1900301360>), <https://doi.org/10.1515/ESRF-DC-1897099390> (<https://paleo.esrf.fr/datasets/1900349982>), <https://doi.org/10.1515/ESRF-DC-1897099398> (<https://paleo.esrf.fr/datasets/1900351006>), <https://doi.org/10.1515/ESRF-DC-1900351106> (<https://paleo.esrf.fr/datasets/1900351393>), <https://doi.org/10.1515/ESRF-DC-1900351114> (<https://paleo.esrf.fr/datasets/1900351634>), <https://doi.org/10.1515/ESRF-DC-1900351122> (<https://paleo.esrf.fr/datasets/1900352175>), <https://doi.org/10.1515/ESRF-DC-1900351130> (<https://paleo.esrf.fr/datasets/1900352562>), <https://doi.org/10.1515/ESRF-DC-1900353418> (<https://paleo.esrf.fr/datasets/1900352627>), <https://doi.org/10.1515/ESRF-DC-1900351138> (<https://paleo.esrf.fr/datasets/1900352628>), <https://doi.org/10.1515/ESRF-DC-1900351146> (<https://paleo.esrf.fr/datasets/1900352692>), <https://doi.org/10.1515/ESRF-DC-1900353004> (<https://paleo.esrf.fr/datasets/1900352755>), <https://doi.org/10.1515/ESRF-DC-1900353012> (<https://paleo.esrf.fr/datasets/1900352845>), <https://doi.org/10.1515/ESRF-DC-1900353028> (<https://paleo.esrf.fr/datasets/1900352960>), <https://doi.org/10.1515/ESRF-DC-1900353036> (<https://paleo.esrf.fr/datasets/1900352968>), <https://doi.org/10.1515/ESRF-DC-1900353044> (<https://paleo.esrf.fr/datasets/1900353143>), <https://doi.org/10.1515/ESRF-DC-1900353402> (<https://paleo.esrf.fr/datasets/1900353216>), <https://doi.org/10.1515/ESRF-DC-1900353410> (<https://paleo.esrf.fr/datasets/1900353287>) and <https://doi.org/10.1515/ESRF-DC-1900353426> (<https://paleo.esrf.fr/datasets/1900353891>).

55. Smith, T. M. et al. Dental evidence for ontogenetic differences between modern humans and Neanderthals. *Proc. Natl Acad. Sci. USA* **107**, 20923–20928 (2010).
56. Le Cabec, A., Tang, N. & Tafforeau, P. Accessing developmental information of fossil hominin teeth using new synchrotron microtomography-based visualization techniques of dental surfaces and interfaces. *PLoS ONE* **10**, e0123019 (2015).
57. McFarlane, G. et al. An inconstant biorhythm: the changing pace of Retzius periodicity in human permanent teeth. *Am. J. Phys. Anthropol.* **175**, 172–186 (2021).
58. Dean, M. C. & Vesev, P. Preliminary observations on increasing root length during the eruptive phase of tooth development in modern humans and great apes. *J. Hum. Evol.* **54**, 258–271 (2008).
59. Dean, M. C. in *Forensic Microscopy for Skeletal Tissues: Methods and Protocols* (ed. Bell, L. S.) 89–100 (Springer, 2012).
60. Antoine, D. & Hillson, S. in *A Companion to Dental Anthropology* (eds Irish, J. D. & Scott, G. R.) 223–243 (Wiley, 2015).
61. Reid, D. J. & Guatelli-Steinberg, D. Updating histological data on crown initiation and crown completion ages in southern Africans. *Am. J. Phys. Anthropol.* **162**, 817–829 (2017).
62. Kuykendall, K. L. & Conroy, G. C. Permanent tooth calcification in chimpanzees (*Pan troglodytes*): patterns and polymorphisms. *Am. J. Phys. Anthropol.* **99**, 159–174 (1996).
63. Smith, B. H. in *Advances in Dental Anthropology* (eds Kelley, M. A. & Larsen, C. S.) 143–168 (Wiley, 1991).
64. AlQahtani, S. J., Hector, M. P. & Liversidge, H. M. Brief communication: the London atlas of human tooth development and eruption. *Am. J. Phys. Anthropol.* **142**, 481–490 (2010).

65. Esan, T. A., Yengopal, V. & Schepartz, L. A. The Demirjian versus the Willems method for dental age estimation in different populations: a meta-analysis of published studies. *PLoS ONE* **12**, e0186682 (2017).
66. Demirjian, A., Goldstein, H. & Tanner, J. M. A new system of dental age assessment. *Hum. Biol.* **45**, 211–227 (1973).
67. Nyström, M. et al. Dental maturity in Finnish children, estimated from the development of seven permanent mandibular teeth. *Acta Odontol. Scand.* **44**, 193–198 (1986).
68. Koshy, S. & Tandon, S. Dental age assessment: the applicability of Demirjian's method in south Indian children. *Forensic Sci. Int.* **94**, 73–85 (1998).
69. Frucht, S., Schnegelsberg, C., Schulte-Mönting, J., Rose, E. & Jonas, I. Dental age in southwest Germany. A radiographic study. *J. Orofac. Orthop.* **61**, 318–329 (2000).
70. Chaillet, N., Nyström, M. & Demirjian, A. Comparison of dental maturity in children of different ethnic origins: international maturity curves for clinicians. *J. Forensic Sci.* **50**, 1164–1174 (2005).
71. Baghdadi, Z. D. Dental maturity in Saudi children using the Demirjian method: a comparative study and new prediction models. *Int. Sch. Res. Notices* **2013**, 390314 (2013).
72. Bunyarit, S. S., Nambiar, P., Naidu, M., Asif, M. K. & Poh, R. Y. Y. Dental age estimation of Malaysian Indian children and adolescents: applicability of Chaillet and Demirjian's modified method using artificial neural network. *Ann. Hum. Biol.* **49**, 192–199 (2022).
73. Shi, L. et al. Dental age estimation of Tibetan children and adolescents: comparison of Demirjian, Willems methods and a newly modified Demirjian method. *Leg. Med.* **55**, 102013 (2022).
74. Boughner, J. C., Dean, M. C. & Wilgenbusch, C. S. Permanent tooth mineralization in bonobos (*Pan paniscus*) and chimpanzees (*P. troglodytes*). *Am. J. Phys. Anthropol.* **149**, 560–571 (2012).
75. Conroy, G. C. & Vannier, M. W. Dental development in South African australopithecines. Part I: Problems of pattern and chronology. *Am. J. Phys. Anthropol.* **86**, 121–136 (1991).
76. Conroy, G. C. & Vannier, M. W. Dental development in South African australopithecines. Part II: Dental stage assessment. *Am. J. Phys. Anthropol.* **86**, 137–156 (1991).
77. Dean, C. et al. Growth and development of the third permanent molar in *Paranthropus robustus* from Swartkrans, South Africa. *Sci. Rep.* **10**, 19053 (2020).
78. Kelley, J. & Schwartz, G. T. Dental development and life history in living African and Asian apes. *Proc. Natl Acad. Sci. USA* **107**, 1035–1040 (2010).
79. Dean, M. C., Liversidge, H. M. & Elamin, F. Combining radiographic and histological data for dental development to compare growth in the past and the present. *Ann. Hum. Biol.* **41**, 336–347 (2014).
80. Smith, B. H. Patterns of dental development in *Homo*, *Australopithecus*, *Pan*, and *Gorilla*. *Am. J. Phys. Anthropol.* **94**, 307–325 (1994).
81. Esan, T. A. & Schepartz, L. A. The WITS atlas: a Black southern African dental atlas for permanent tooth formation and emergence. *Am. J. Phys. Anthropol.* **166**, 208–218 (2018).
82. Nyström, E. M., Ranta, M. H., Peltola, S. J. & Kataja, M. J. Timing of developmental stages in permanent mandibular teeth of Finns from birth to age 25. *Acta Odontol. Scand.* **65**, 36–43 (2007).
83. Smith, T. M. et al. Earliest evidence of modern human life history in North African early *Homo sapiens*. *Proc. Natl Acad. Sci. USA* **104**, 6128–6133 (2007).
84. Nimkulrat, S., Panichuttra, A., Ratisoontom, C. & Porntaveetus, T. Evaluation of dens evaginatus by CBCT and exome sequencing in Thai population. *J. Dent. Assoc. Thai* **72**, 500–508 (2022).
85. Martelli, S. A. in *Spinal Evolution: Morphology, Function, and Pathology of the Spine in Hominoid Evolution* (eds Been, E. et al.) 247–281 (Springer, 2019).

**Acknowledgements** Support was provided by European Synchrotron Radiation Facility (ESRF) grants EC-022 and EC-767 to C.P.E.Z., P.T., M.S.P.d.L. and D.L., by Swiss National Science Foundation grant CR3213\_166053 to C.P.E.Z., and by an open-access publication grant from the Dietrich-Schindler-Stiftung. Support to D.L. was provided by the Georgian National Science Foundation, the National Geographic Society and the L.S.B. Leakey Foundation.

**Author contributions** C.P.E.Z., M.S.P.d.L. and P.T. designed the research. D.L. contributed the fossil specimens. P.T. acquired and processed the synchrotron data. V.B. and P.T. analysed the synchrotron data. V.B., M.S.P.d.L. and C.P.E.Z. analysed the comparative data. C.P.E.Z., M.S.P.d.L., V.B. and P.T. wrote the manuscript.

**Competing interests** The authors declare no competing interests.

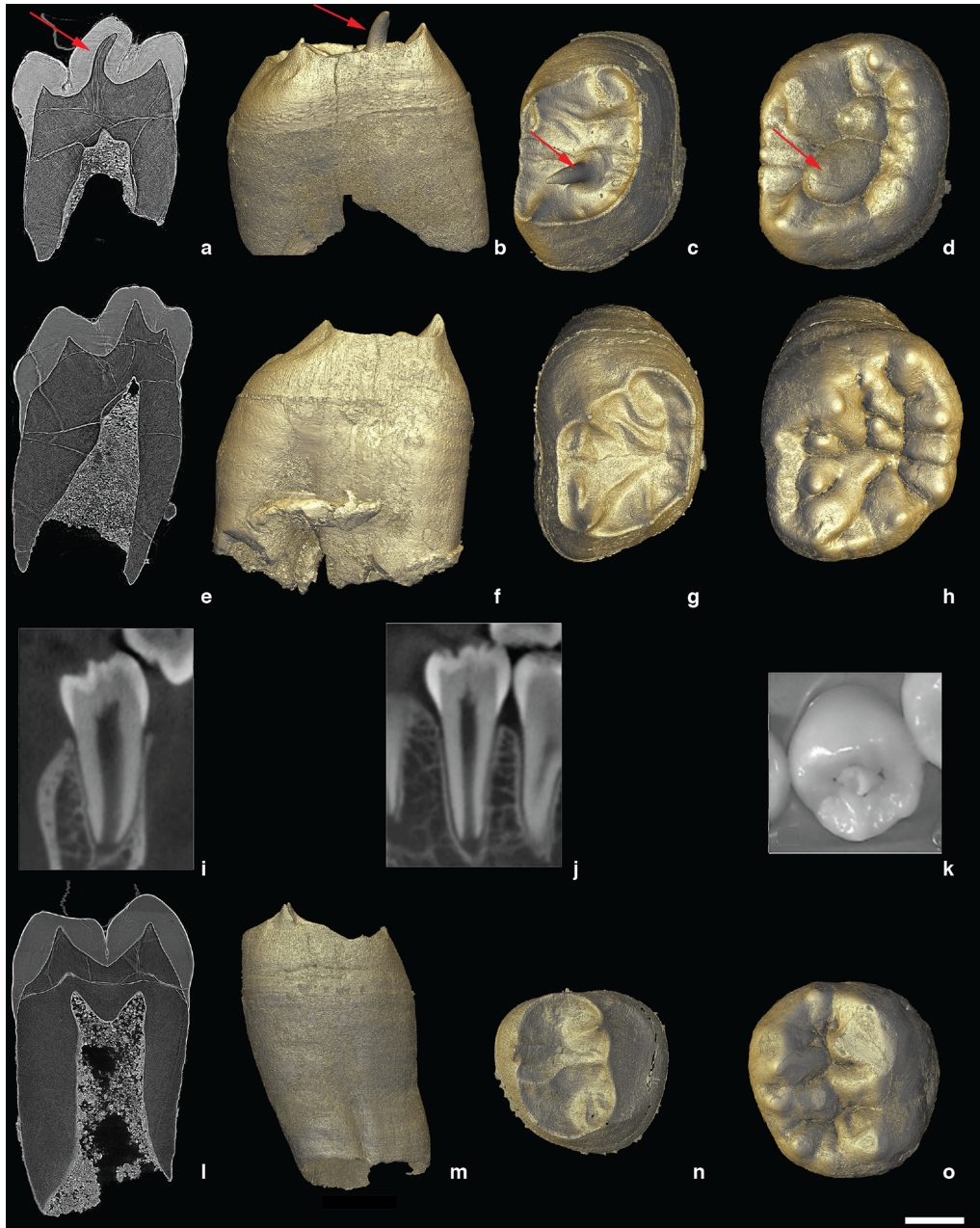
## Additional information

**Supplementary information** The online version contains supplementary material available at <https://doi.org/10.1038/s41586-024-08205-2>.

**Correspondence and requests for materials** should be addressed to Christoph P. E. Zollikofer, Paul Tafforeau or Marcia S. Ponce de León.

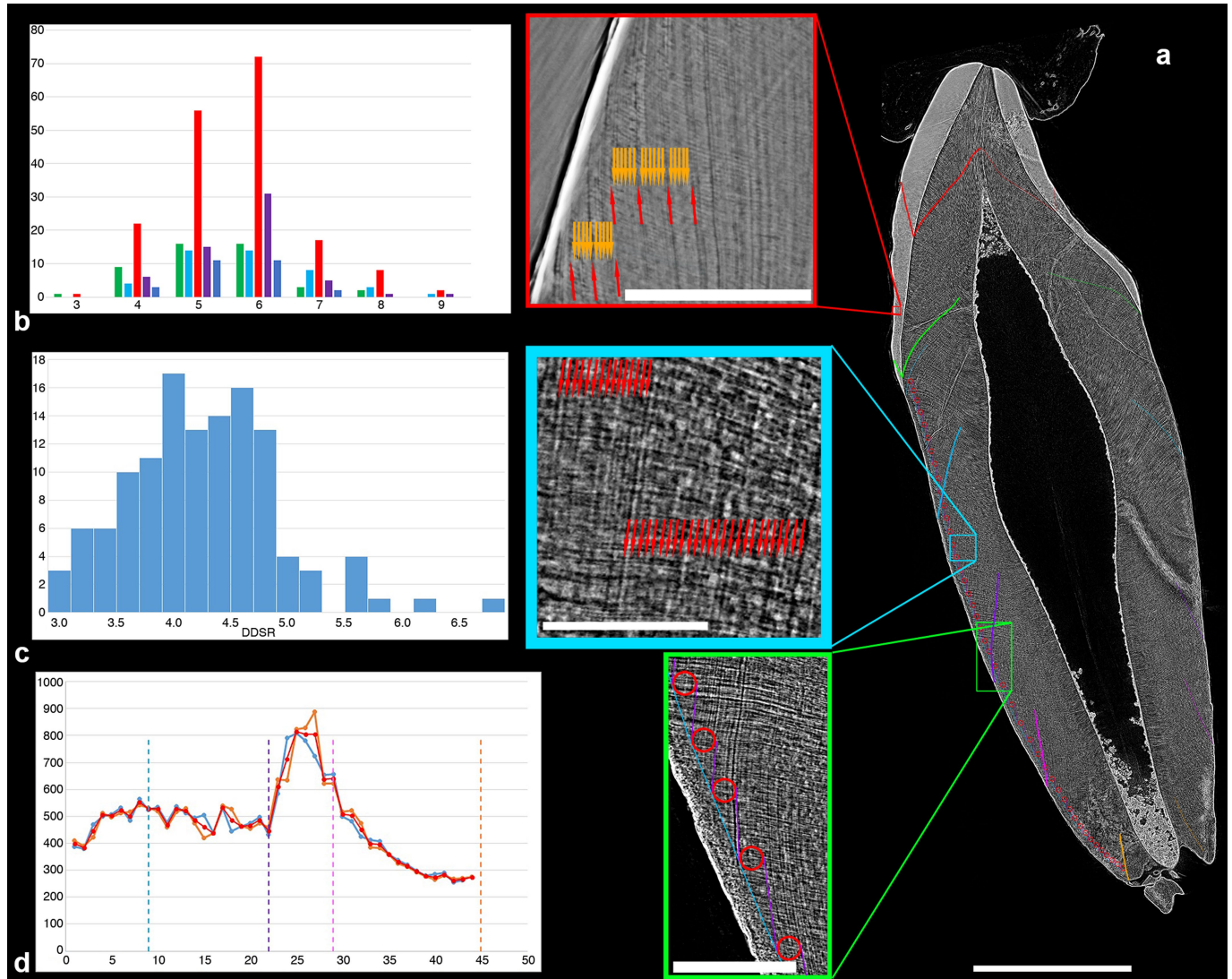
**Peer review information** Nature thanks Debbie Guatelli-Steinberg, Kevin Kuykendall and the other, anonymous, reviewer(s) for their contribution to the peer review of this work. Peer reviewer reports are available.

**Reprints and permissions information** is available at <http://www.nature.com/reprints>.



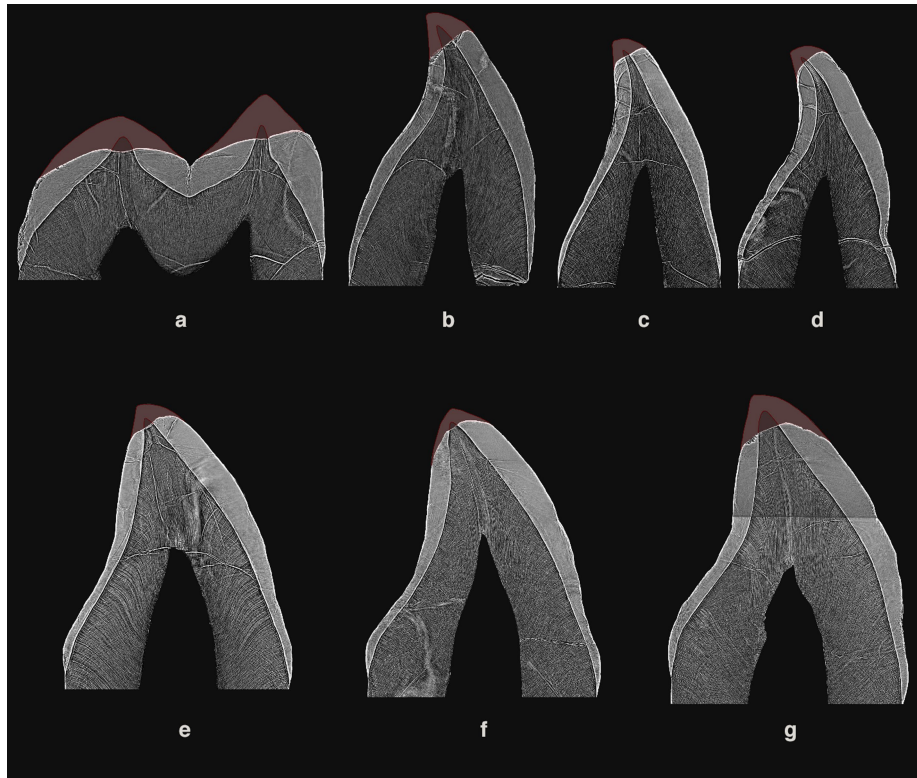
**Extended Data Fig. 1 | Dmanisi and human third molars.** **a-d:** D2711 upper right third molar (URM3) with supernumerary central cusp ("*dense evaginatus*"). **a:** Mesial view of bucco-lingual cross-section; **b:** buccal view of the dentinal structures of the root and crown (enamel digitally removed); **c:** occlusal view of the enamel-dentin junction (EDJ); **d:** occlusal view of the crown surface (enamel). **e-h:** D2700 upper left third molar (ULM3) with standard morphology. All views are mirror images to facilitate comparison with D2711 URM3. **e:** Mesial view of bucco-lingual cross-section; **f:** buccal view of the dentinal structures of the root and crown (enamel digitally removed); **g:** occlusal view of the EDJ;

**h:** occlusal view of the crown surface (enamel). **i-k:** Supernumerary cusp similar to D2711 in a modern human lower left second premolar (LLP4); coronal and sagittal cross-sections (dental cone beam CT), and occlusal view. **l-o:** D2735 lower right third molar (LRM3) with standard morphology. **l:** Mesial view of bucco-lingual cross-section; **m:** buccal view of the dentinal structures of the root and crown (enamel digitally removed); **n:** occlusal view of the EDJ; **o:** occlusal view of the crown surface (enamel). Scale bar is 3 mm. Images in **i-k** reproduced with permission from ref. 84, Journal of the Dental Association of Thailand.

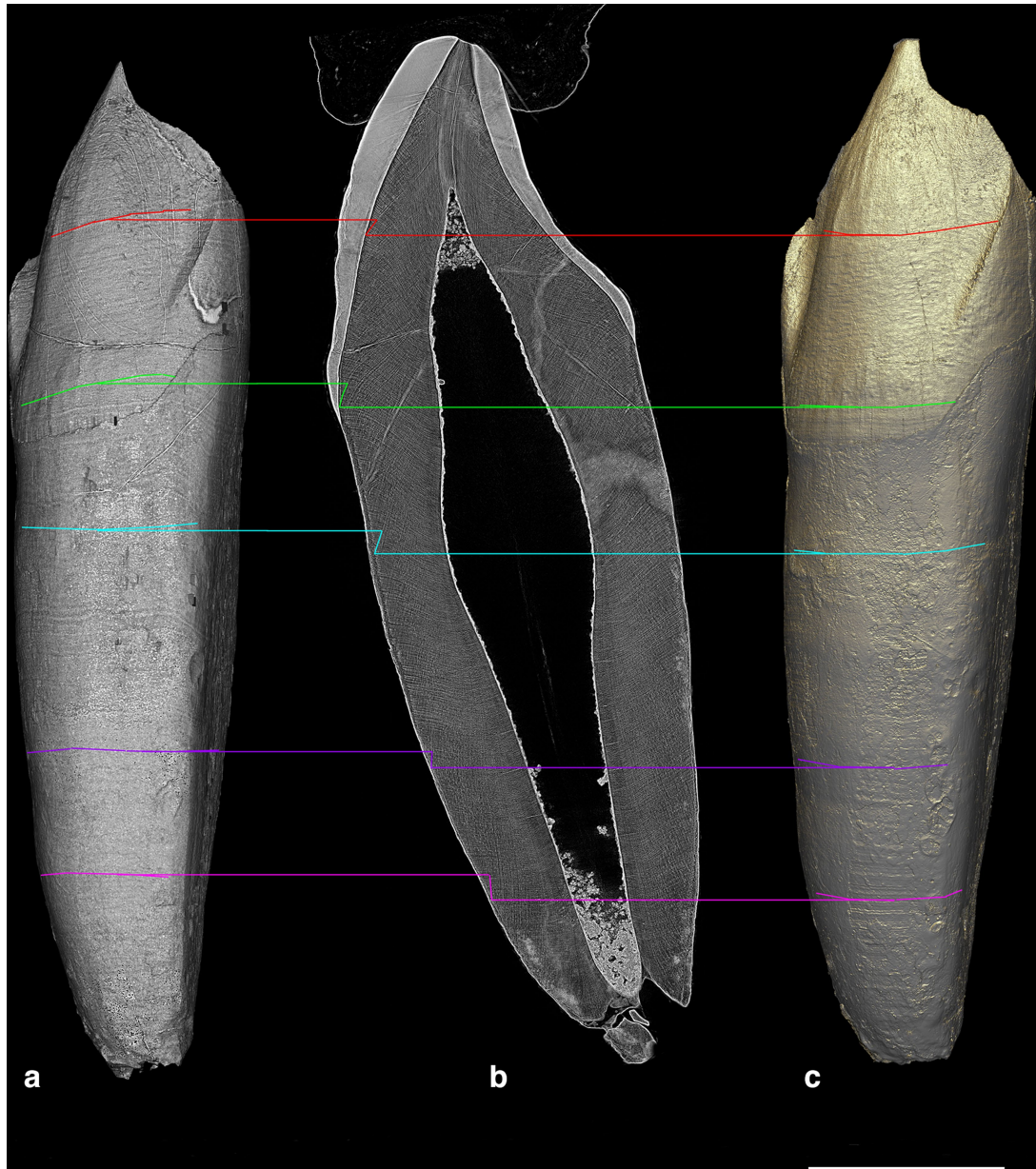


**Extended Data Fig. 2 | Short-periodicity and long-periodicity measurements.** **a:** Labio-lingual cross section through the upper right canine (URC) of D2700; scale bar is 6 mm. **b:** Daily enamel secretion structures (cross striations/laminations, yellow arrows) and long-periodicity structures (Retzius lines, red arrows); scale bar is 0.2 mm. The histogram shows the distribution of the  $N = 177$  long-periodicity duration counts (see SI Data 2); colour bars represent total number of counts (red), and counts for individual teeth (green: URC; light blue: URP4; purple: ULM3; dark blue: LRM3). **c:** Long-period Andresen lines (red arrows) in the root; scale bar is 0.5 mm. The histogram

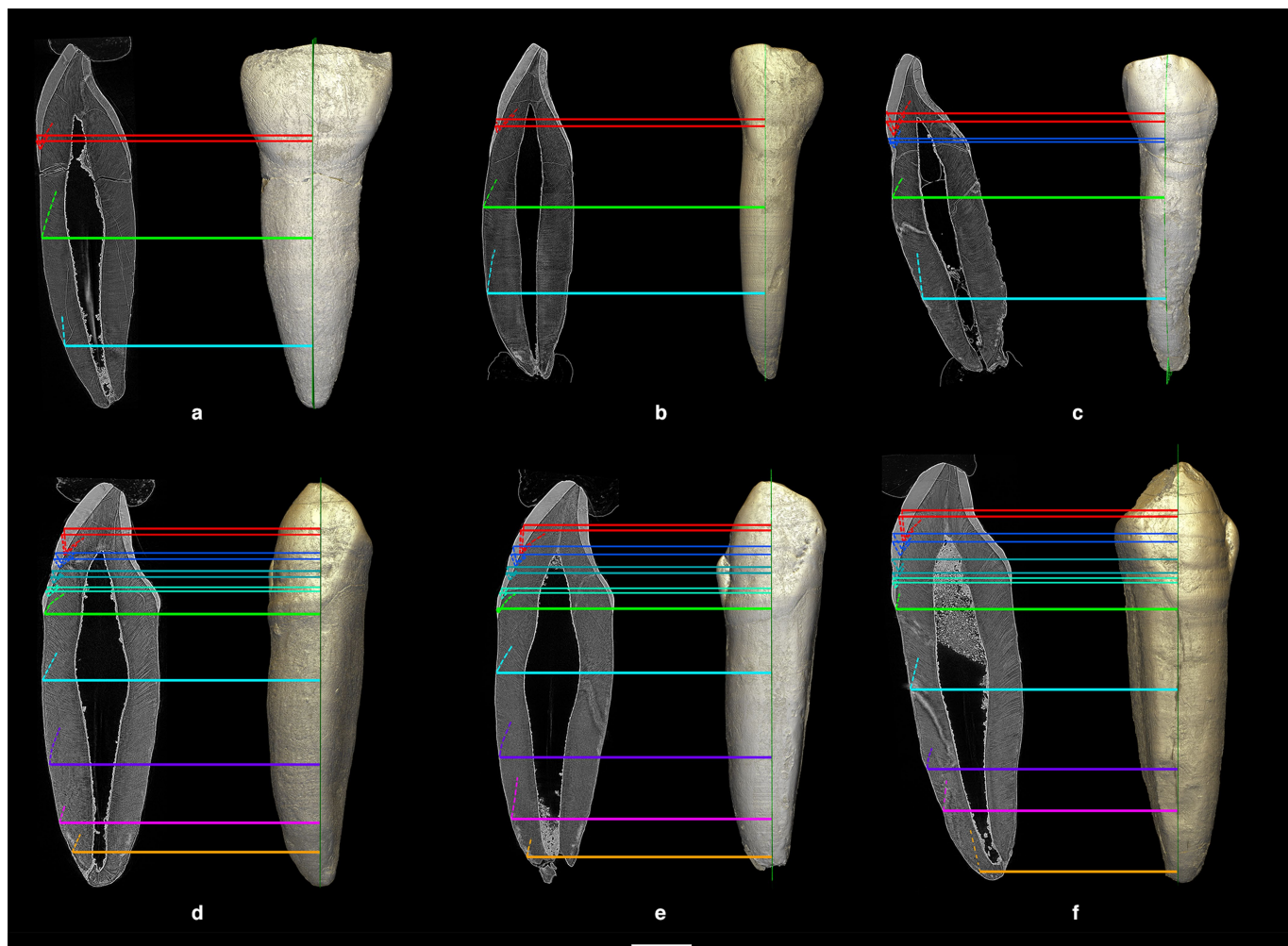
shows the distribution of the  $N = 124$  long-period dentin secretion rate measurements, which when multiplied by the periodicity gives the daily dentin secretion rate (DDSR in  $\mu\text{m}/\text{day}$ ; bin width is  $0.2 \mu\text{m}/\text{day}$ ) (see SI Data 3). **d:** Method of measuring the root extension rate; scale bar is 1 mm; red circles are 200  $\mu\text{m}$  in diameter; pink lines extend from circle to cemento-dentin junction (blue). The graph shows the root extension rate profile for three independent measurements (x-axis: consecutive measurement intervals corresponding to the red circles in **a**; y-axis: root extension rate in  $\mu\text{m}$  per interval). Colours of stress lines as in Fig. 2.



**Extended Data Fig. 3 | Reconstruction of worn dental cusps of D2700/D2735.** Dark red areas represent reconstructed cusp tips and dentin horn tips. **a:** ULM1; **b:** UR11; **c:** LR12; **d:** UL12; **e:** LLC; **f:** URC; **g:** LRC.

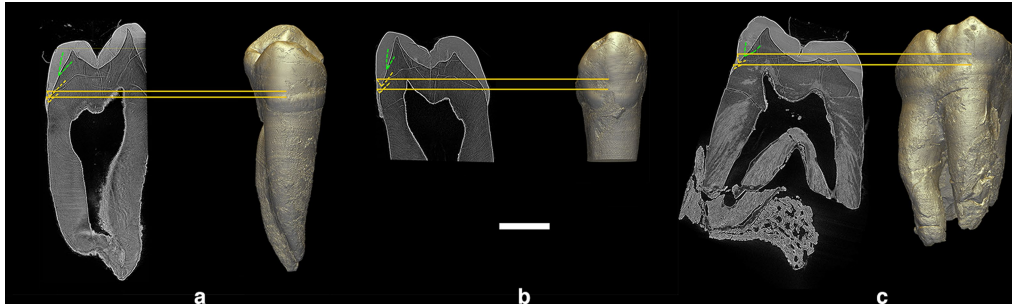


**Extended Data Fig. 4 | Stress line identification on the upper right canine (URC) of D2700.** **a:** Digitally eroded dentin surface of the root and crown (methods see ref. 56). **b:** Labio-lingual cross-sectional slice. **c:** Non-eroded dentin surface. Colours of stress lines as Fig. 2; scale bar is 6 mm.



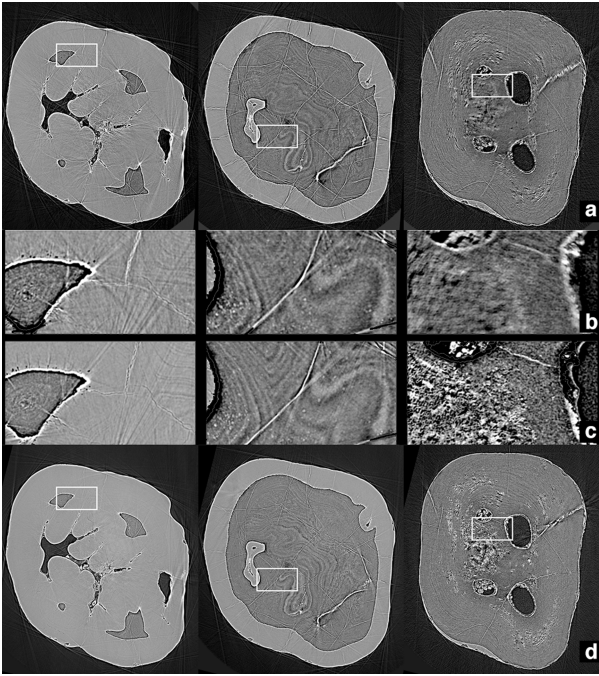
**Extended Data Fig. 5 | Matching of hypoplasias across the anterior teeth of D2700/D2735.** a: URI1; b: LRI2; c: ULI2; d: LLC; e: URC; f: LRC. Each tooth is displayed as a labio-lingual virtual cross section and as a 3D reconstruction of

its external surface. Horizontal solid lines indicate lower and upper bounds of hypoplasia; dashed lines follow hypoplasias into enamel and dentin. Colours of stress lines as in Fig. 2; scale bar is 5 mm.

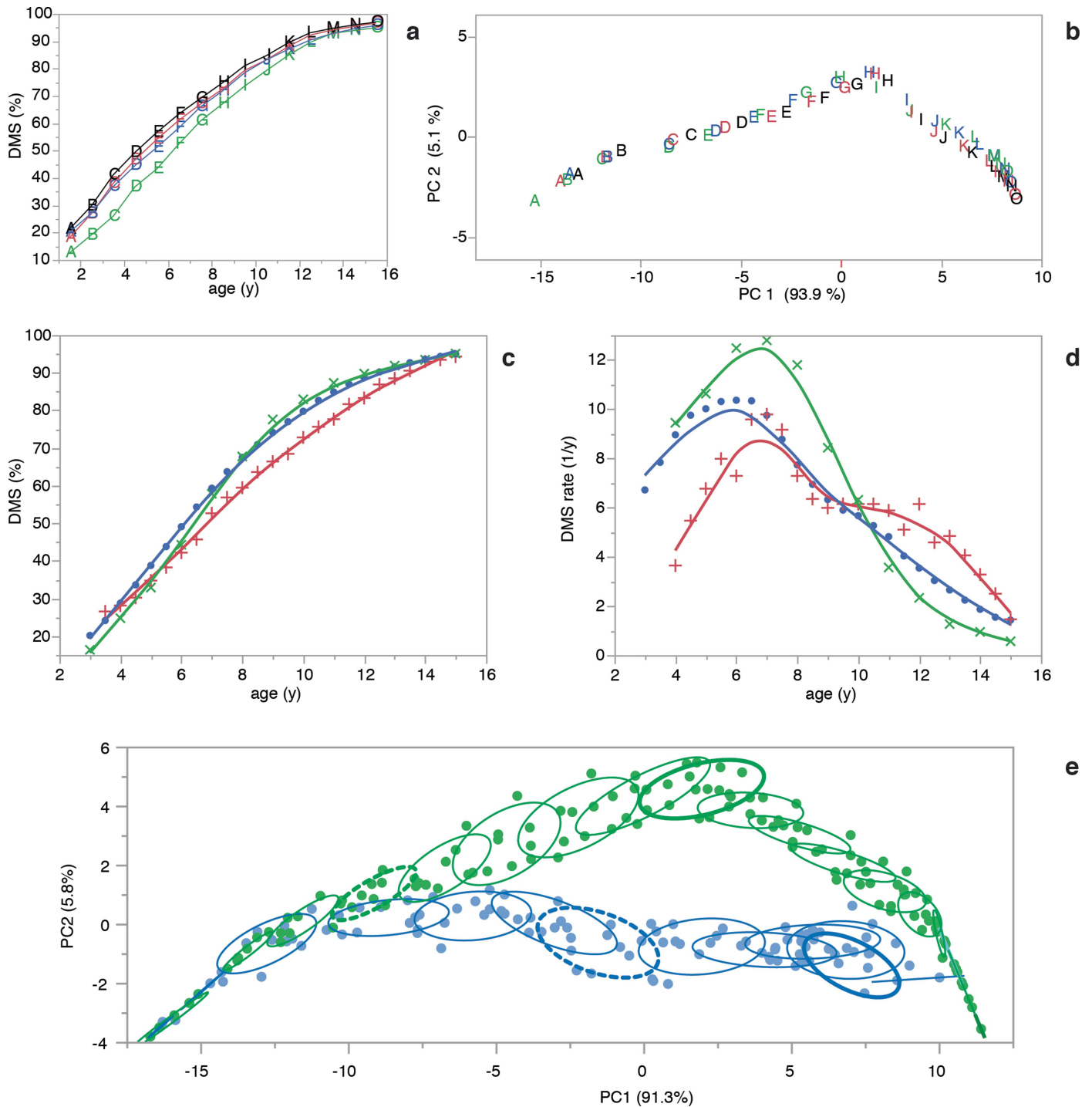


**Extended Data Fig. 6 | Matching of hypoplasias across the premolars and second molar of D2700. a:** URP3; **b:** URP4; **c:** ULM2. Each tooth is displayed as a labio-lingual virtual cross section and as a 3D reconstruction of its external

surface. Horizontal solid lines indicate lower and upper bounds of hypoplasia; dashed lines follow hypoplasia into enamel and dentin. Colour of stress line as in Fig. 2; scale bar is 5 mm.



**Extended Data Fig. 7 | Quality comparison between monochromatic and polychromatic scans on the ULM2.** **a-b:** Data from the 2009 experimental session, obtained with a monochromatic beam set at 51 keV with 5 m of propagation using a gadox 5  $\mu\text{m}$  scintillator. The scan took about 12 h, and the dentin tends to diffuse the beam, resulting in a local decohesion effect that blurs the middle of the slices at the level of the cervix. **a:** Horizontal slices of ULM2 at different levels in the crown. **b:** Detail of slices from **a**. **c-d:** Data from the 2012 experimental session obtained with a polychromatic beam with an effective energy of 64 keV, using the same detector and 5 m of propagation, but with a LuAG:Ce 100  $\mu\text{m}$  scintillator. The scan took about 2 h, and the decohesion effect has completely disappeared thanks to the higher energy. **d:** Horizontal slices of ULM2 at the same location as in **a**. **c:** Detail of slices from **d**.



**Extended Data Fig. 8 | Data standardization and consistency tests. a and b:** Influence of scoring schemes and imaging modalities on the dental maturation trajectories of Finnish children. Blue: original 8-stage radiography-based DMS data from Nyström07<sup>82</sup>. Green: original 10-stage radiography-based DMS data from Haavikko70<sup>40</sup>. Red: Haavikko70 radiography-based data recoded to 8-stage system. Black: Haavikko70 data recoded to (simulated) histological 8-stage scores (using the conversion tables provided in ref. 13). **a:** DMS of the total dentition (I1-M3) versus age in years. **b:** DMS-PCA of the maturation data of all teeth at given ages (A-O: 1.5-15.5 years in 1-year intervals). Graph **a** shows that recoding of the original Haavikko70 data (green → red) results in good correspondence with the Nyström07 data (blue). Virtual histology-based DMS scores (black) are consistently more advanced than radiography-based scores (red). Graph **b** shows that all trajectories through DMS-PCA space largely coincide, but differ in advancement along the trajectory for any given age.

**c and d:** Total DMS profiles of three different samples of Finnish children. Red: data from Haavikko70<sup>40</sup> (10-stage DMS system, all 8 teeth [I1-M3]). Green: data from Nyström86<sup>67</sup> (8-stage DMS system, 7 teeth [I1-M2]). Blue: data from Nyström07<sup>82</sup> (8-stage system, all 8 teeth). **c:** DMS vs. age in years. **d:** DMS instantaneous rate vs. age in years. Although DMS profiles and DMS rate values differ between studies, the timing of the rate peaks (dentition growth spurt, DGS) is similar: at -6 years in the most recent sample (Nyström07) and at -7 years in the earlier samples (Haavikko70 and Nyström86). **e:** DMS-PCA on I1-M3 dental maturation data of known-age humans (green) and chimpanzees (blue). Density ellipses (1sdev) are drawn around 1-year age classes. Dashed and bold ellipses represent distributions at 5 years and 10 years of age, respectively. Note that the natural variation within age classes is similar in magnitude to the uncalibrated method-dependent variation within age classes (**b**).

**Extended Data Table 1 | Dentition growth spurt (DGS) in human populations**

| sample                   | <i>N</i> | DGS (years) | teeth | reference |
|--------------------------|----------|-------------|-------|-----------|
| Finland                  | 1162     | 6.8         | I1-M3 | 40        |
| European                 | >500     | 7.0         | I1-M3 | 63        |
| UK, Bangladesh           | 704      | 7.5         | I1-M3 | 64        |
| S-Africa                 | 642      | 7.0         | I1-M3 | 81        |
| Canada                   | 2928     | 7.5         | I1-M2 | 66        |
| Finland                  | 248      | 7.0         | I1-M2 | 67        |
| Finland                  | 1970     | 6.0         | I1-M3 | 82        |
| S India                  | 184      | 7.5         | I1-M2 | 68        |
| Germany                  | 1003     | 6.0         | I1-M2 | 69        |
| Europe, N-America, Korea | 9577     | 8.3         | I1-M2 | 70        |
| Saudi Arabia             | 422      | 6.5         | I1-M2 | 71        |
| Malaysia                 | 1015     | 8.5         | I1-M2 | 72        |
| Tibet                    | 1951     | 8.0         | I1-M2 | 73        |
| average                  |          | 7.4         |       |           |

Extended Data Table 2 | Dmanisi postcranial epiphyseal fusion stage, and comparative human and chimpanzee data

|                | Dmanisi fusion state                   | chimpanzee age (years) at |                 | human age (years) at |                 | references |
|----------------|--|---------------------------|-----------------|----------------------|-----------------|------------|
|                |  | midfusion                 | complete fusion | midfusion females    | midfusion males |            |
| distal humerus | incomplete fusion of medial epicondyle | 6.3                       | 9.2             | 12                   | 15              | 22, 46     |
| humeral head   | epiphyseal plate unfused               | 9.1                       | >9.5            | 16                   | 19              | 22, 46     |
| vertebrae      | annular epiphyses unfused              | 9                         | >11             | 18                   | 18.9            | 22, 85     |
| phalanges      | epiphyses fused                        | 8.5                       | >9.45           | 11-13                | 14-16           | 22, 46     |
| metatarsal I   | epiphyseal fusion incomplete           | 8.9                       | >9.45           | 13-15                | 16-18           | 22, 46     |
| metatarsal IV  | epiphyses fused                        | 9.0                       | >9.45           | 11-13                | 14-16           | 22, 46     |

See refs. 22,46,85.

Reporting Summary

Nature Portfolio wishes to improve the reproducibility of the work that we publish. This form provides structure for consistency and transparency in reporting. For further information on Nature Portfolio policies, see our [Editorial Policies](#) and the [Editorial Policy Checklist](#).

Statistics

For all statistical analyses, confirm that the following items are present in the figure legend, table legend, main text, or Methods section.

|                                     |  |
|-------------------------------------|--|
| n/a                                 | Confirmed  |
| <input type="checkbox"/>            | <input checked="" type="checkbox"/> The exact sample size ( <i>n</i> ) for each experimental group/condition, given as a discrete number and unit of measurement   |
| <input checked="" type="checkbox"/> | <input type="checkbox"/> A statement on whether measurements were taken from distinct samples or whether the same sample was measured repeatedly   |
| <input type="checkbox"/>            | <input checked="" type="checkbox"/> The statistical test(s) used AND whether they are one- or two-sided<br><i>Only common tests should be described solely by name; describe more complex techniques in the Methods section.</i>   |
| <input checked="" type="checkbox"/> | <input type="checkbox"/> A description of all covariates tested  |
| <input checked="" type="checkbox"/> | <input type="checkbox"/> A description of any assumptions or corrections, such as tests of normality and adjustment for multiple comparisons   |
| <input type="checkbox"/>            | <input checked="" type="checkbox"/> A full description of the statistical parameters including central tendency (e.g. means) or other basic estimates (e.g. regression coefficient) AND variation (e.g. standard deviation) or associated estimates of uncertainty (e.g. confidence intervals) |
| <input type="checkbox"/>            | <input checked="" type="checkbox"/> For null hypothesis testing, the test statistic (e.g. <i>F</i> , <i>t</i> , <i>r</i> ) with confidence intervals, effect sizes, degrees of freedom and <i>P</i> value noted<br><i>Give P values as exact values whenever suitable.</i>                     |
| <input checked="" type="checkbox"/> | <input type="checkbox"/> For Bayesian analysis, information on the choice of priors and Markov chain Monte Carlo settings  |
| <input checked="" type="checkbox"/> | <input type="checkbox"/> For hierarchical and complex designs, identification of the appropriate level for tests and full reporting of outcomes  |
| <input checked="" type="checkbox"/> | <input type="checkbox"/> Estimates of effect sizes (e.g. Cohen's <i>d</i> , Pearson's <i>r</i> ), indicating how they were calculated  |

Our web collection on [statistics for biologists](#) contains articles on many of the points above.

Software and code

Policy information about [availability of computer code](#)

|                 |                            |
|-----------------|----------------------------|
| Data collection | VGStudioMax v3.4           |
| Data analysis   | MS Excel v16.16, JMP v15.2 |

For manuscripts utilizing custom algorithms or software that are central to the research but not yet described in published literature, software must be made available to editors and reviewers. We strongly encourage code deposition in a community repository (e.g. GitHub). See the Nature Portfolio [guidelines for submitting code & software](#) for further information.

Data

Policy information about [availability of data](#)

All manuscripts must include a [data availability statement](#). This statement should provide the following information, where applicable:

- Accession codes, unique identifiers, or web links for publicly available datasets
- A description of any restrictions on data availability
- For clinical datasets or third party data, please ensure that the statement adheres to our [policy](#)

All the synchrotron data used in this study are available on the ESRF Palaeontology Database:  
<https://doi.org/10.1515/ESRF-DC-1897099374> (<https://paleo.esrf.fr/datasets/1900295870>)  
<https://doi.org/10.1515/ESRF-DC-1897099382> (<https://paleo.esrf.fr/datasets/1900301360>)  
<https://doi.org/10.1515/ESRF-DC-1897099390> (<https://paleo.esrf.fr/datasets/1900349982>)

<https://doi.org/10.15151/ESRF-DC-1897099398> (<https://paleo.esrf.fr/datasets/1900351006>)  
<https://doi.org/10.15151/ESRF-DC-1900351106> (<https://paleo.esrf.fr/datasets/1900351393>)  
<https://doi.org/10.15151/ESRF-DC-1900351114> (<https://paleo.esrf.fr/datasets/1900351634>)  
<https://doi.org/10.15151/ESRF-DC-1900351122> (<https://paleo.esrf.fr/datasets/1900352175>)  
<https://doi.org/10.15151/ESRF-DC-1900351130> (<https://paleo.esrf.fr/datasets/1900352562>)  
<https://doi.org/10.15151/ESRF-DC-1900353418> (<https://paleo.esrf.fr/datasets/1900352627>)  
<https://doi.org/10.15151/ESRF-DC-1900351138> (<https://paleo.esrf.fr/datasets/1900352628>)  
<https://doi.org/10.15151/ESRF-DC-1900351146> (<https://paleo.esrf.fr/datasets/1900352692>)  
<https://doi.org/10.15151/ESRF-DC-1900353004> (<https://paleo.esrf.fr/datasets/1900352755>)  
<https://doi.org/10.15151/ESRF-DC-1900353012> (<https://paleo.esrf.fr/datasets/1900352845>)  
<https://doi.org/10.15151/ESRF-DC-1900353028> (<https://paleo.esrf.fr/datasets/1900352960>)  
<https://doi.org/10.15151/ESRF-DC-1900353036> (<https://paleo.esrf.fr/datasets/1900352968>)  
<https://doi.org/10.15151/ESRF-DC-1900353044> (<https://paleo.esrf.fr/datasets/1900353143>)  
<https://doi.org/10.15151/ESRF-DC-1900353402> (<https://paleo.esrf.fr/datasets/1900353216>)  
<https://doi.org/10.15151/ESRF-DC-1900353410> (<https://paleo.esrf.fr/datasets/1900353287>)  
<https://doi.org/10.15151/ESRF-DC-1900353426> (<https://paleo.esrf.fr/datasets/1900358391>)

## Research involving human participants, their data, or biological material

Policy information about studies with [human participants or human data](#). See also policy information about [sex, gender \(identity/presentation\), and sexual orientation](#) and [race, ethnicity and racism](#).

Reporting on sex and gender N/A

Reporting on race, ethnicity, or other socially relevant groupings N/A

Population characteristics N/A

Recruitment N/A

Ethics oversight N/A

Note that full information on the approval of the study protocol must also be provided in the manuscript.

## Field-specific reporting

Please select the one below that is the best fit for your research. If you are not sure, read the appropriate sections before making your selection.

☒ Life sciences ☐ Behavioural & social sciences ☐ Ecological, evolutionary & environmental sciences

For a reference copy of the document with all sections, see [nature.com/documents/nr-reporting-summary-flat.pdf](https://www.nature.com/documents/nr-reporting-summary-flat.pdf)

## Life sciences study design

All studies must disclose on these points even when the disclosure is negative.

Sample size fossil sample size: N=1 (D2700/D2735); sample size limited by availability of fossil specimens

Data exclusions Data of URM3 excluded: this tooth has an unusual supernumerary cusp.

Replication N=2 independent reconstructions of D2700/D2735 dental ontogeny by V.B. and P.T.; data in SI Data 1  
N= 177 independent measures performed to estimate long-periodicity value; data in SI Data 2  
N=124 independent measures performed to estimate daily dentin secretion rate; data in SI Data 3

Randomization N/A

Blinding The analyses performed by V.B. and P.T. were blinded to each other.

## Reporting for specific materials, systems and methods

We require information from authors about some types of materials, experimental systems and methods used in many studies. Here, indicate whether each material, system or method listed is relevant to your study. If you are not sure if a list item applies to your research, read the appropriate section before selecting a response.

## Materials &amp; experimental systems

## Methods

|                                     |   |
|-------------------------------------|---|
| n/a                                 | Involvement in the study  |
| <input checked="" type="checkbox"/> | <input type="checkbox"/> Antibodies                               |
| <input checked="" type="checkbox"/> | <input type="checkbox"/> Eukaryotic cell lines                    |
| <input type="checkbox"/>            | <input checked="" type="checkbox"/> Palaeontology and archaeology |
| <input checked="" type="checkbox"/> | <input type="checkbox"/> Animals and other organisms              |
| <input checked="" type="checkbox"/> | <input type="checkbox"/> Clinical data                            |
| <input checked="" type="checkbox"/> | <input type="checkbox"/> Dual use research of concern             |
| <input checked="" type="checkbox"/> | <input type="checkbox"/> Plants                                   |

|                                     |   |
|-------------------------------------|---|
| n/a                                 | Involvement in the study                        |
| <input checked="" type="checkbox"/> | <input type="checkbox"/> ChIP-seq               |
| <input checked="" type="checkbox"/> | <input type="checkbox"/> Flow cytometry         |
| <input checked="" type="checkbox"/> | <input type="checkbox"/> MRI-based neuroimaging |

## Palaeontology and Archaeology

|                          |  |
|--------------------------|--|
| Specimen provenance      | Dmanisi, Georgia   |
| Specimen deposition      | All Dmanisi specimens are deposited at the Georgian National Museum, Tbilisi, Georgia                                  |
| Dating methods           | N/A  |
| <input type="checkbox"/> | Tick this box to confirm that the raw and calibrated dates are available in the paper or in Supplementary Information. |
| Ethics oversight         | Swiss National Science Foundation, SCOPES program  |

Note that full information on the approval of the study protocol must also be provided in the manuscript.